Strongly Interacting Quantum Gases in One Dimension

Timothy Skaras
Advisor: Professor Han Pu

A thesis completed for the degree of
Bachelor of Science in Computational Physics

Department of Physics and Astronomy
Rice University
Houston, TX
23 April 2019

Contents

1 Introduction

Quantum many-body physics deals with physical systems that contain a large number of interacting particles. In general, these systems are very difficult to study in three spatial dimensions. One-dimensional systems have been the subject of both theoretical and experimental interest in the past decades. Quantum effects and correlations are often more pronounced in low-dimensional geometries. In particular, our work will focus on the phenomenon of dynamical fermionization and the relationship between the large momentum tail for strongly-interacting gases and the Tan Contact.

One example is the Tonks-Girardeau gas, a 1D system of spinless bosons with infinite contact interaction that was proposed and studied over 50 years ago [6, 14] and was realized experimentally more recently [20, 13] using ultracold atoms. The strong, repulsive interaction between these bosons prevents them from occupying the same position, thus giving them similar properties to fermions. In subsection 2.3, we will calculate the density profile in momentum space for this system to study the Tan Contact.

In subsection 2.4, we will consider ultracold, spinless anyons or anyonic Tonks-Girardeau gas. Anyons are particles with wave functions that pick up a complex phase under permutation of particle coordinates. In three dimensions, experimental evidence supports the symmetrization postulate, which holds that wave functions of identical particles are either symmetric (bosons) or antisymmetric (fermions) under particle exchange [8]. Nonetheless, in a system of 1D strongly-interacting, identical particles it has been shown that wave functions that are neither completely symmetric nor antisymmetric are physically allowed [7]. Indeed, there have been applications of anyonic systems in various areas of condensed matter [19, 2].

Next, in section 3 we consider whether these results for spinless systems will still hold when the particles are given a spin degree of freedom. We will perform explicit calculations for two-particle states with different spin configurations. We find that dynamical fermionization will still occur in strongly-interacting spin gases, and we will present a proof by Shah Saad Alam that dynamical fermionization will occur in spin gases with arbitrary particle number.

Lastly, in section 4, we examine more carefully what the necessary components are for dynamical fermionization to occur. We will consider two spinless particles that are confined in an anharmonic trapping potential. Using numerical calculations, we find that dynamical fermionization will still occur in these systems, even if the trapping potential is not symmetric. These results combined with our work on spin gases demonstrate that dynamical fermionization is a more general phenomenon than was previously thought.

2 Spinless Gas

2.1 Introduction

In subsection 2.3, we will calculate the Tan Contact for two hard-core bosons. The Tan Contact originates from the Tan relations derived by Shina Tan in 2008 [24, 23, 22]. These Tan relations applied to a 3D Fermi gas with two spin components and a scattering length that was large relative to the interaction range. The Tan relations involved an extensive quantity known as the Tan contact C, which is associated with different properties of the system. It appears in the coefficient for momentum distribution tails of each spin state but is also associated with the energy of the system in, for instance, the adiabatic sweep theorem [29]. More recently, work has been done on the Tan contact of 1D Bose gas in the Tonks-Girardeau regime [25]. In subsection 2.4, we will look at how these results can be extended to anyonic Tonks-Girardeau gases as well.

We will also explore a phenomenon known as dynamical fermionization. When a strongly-interacting gas undergoes a one-dimensional expansion (i.e., the trapping potential is turned off), the momentum distribution will asymptotically approach the momentum distribution of spinless fermions. This phenomenon was first explored in the context of a Tonks-Girardeau gas [16, 21] but has also been shown to occur in anyonic Tonks-Girardeau gases as well [4]. Our work in this section confirms these results on dynamical fermionization of hard-core anyons.

2.2 Background

We consider ultracold particles in one spatial dimension confined in a harmonic trap. We say these particles have a hard core if they have an interaction which ensures they cannot occupy the same point. In natural units ($\hbar = m = \omega = 1$), the Hamiltonian for a system with this interaction is given by

$$H = H_0 + H_{int} = \sum_{i=1}^{N} -\frac{1}{2}\frac{\partial^2}{\partial x_i^2} + \frac{1}{2}x_i^2 + g \sum_{1\le i<j\le N} \delta(x_i - x_j) \tag{1}$$

where N is the number of particles and $g \to \infty$ is the hard core limit. When g is large but not infinite, the particles have a strong, contact interaction but not a hard core. For the single particle case, quantum harmonic oscillator solutions are [11]

$$\varphi_j(x) = \frac{1}{\pi^{1/4}\sqrt{2^j j!}} H_j(x) e^{-\frac{1}{2}x^2} \qquad \text{for } j = 0, 1, 2, \ldots \tag{2}$$

which can then be used to construct the N particle wave function $\Psi(x_1, \ldots, x_N)$ with the slater determinant or permanent for fermions or bosons respectively. With $\Psi(x_1, \ldots, x_N)$ we can calculate the one-body density matrix (OBDM) $\rho(x, x')$. For N spinless particles it is defined as

$$\rho(x, x') = \int dx_2 \cdots dx_N \Psi^*(x, \ldots, x_N)\Psi(x', \ldots, x_N) \tag{3}$$

where integrals are assumed to go from $-\infty$ to ∞ unless otherwise stated. The OBDM is useful for calculating one body correlations and understanding one body physics. The single-particle real space density profile (RSDP) describes the number density of particles in position space and is defined as

$$n(x) = N\rho(x, x) \tag{4}$$

The single-particle momentum distribution or momentum space density profile (MSDP) is

$$n(p) = \frac{N}{2\pi} \int dx \int dx' e^{ip(x-x')} \rho(x, x') \tag{5}$$

and similarly describes the number density of particles in momentum space.

2.3 Spinless Bosons

2.3.1 Bose-Fermi Mapping

Bosons and fermions have different physical behavior due to their differing exchange properties. Because the fermion wave function is antisymmetric, it will always vanish whenever two fermions occupy the same position. Similarly, the wave function for two hard-core bosons (HCB) will also vanish because of the infinite

interaction. Due to this similarity, this phenomenon of hard-core bosons is known as fermionization. In 1960, Girardeau [6] showed that there was a mapping between systems of fermions and hard-core bosons. This bose-fermi mapping gave a procedure for transforming the wave function Ψ_F for a system of fermions into the wave function Ψ_B for a system of hard-core bosons with the same trapping potential. This powerful technique can be used to study the momentum distribution properties of hard-core bosons.

Let $\Psi_F(x_1, \ldots, x_n)$ be an antisymmetric wave function satisfying the Schrödinger equation for a one-dimensional system of fermions. Girardeau showed that the antisymmetric function A defined as

$$A(x_1, \ldots, x_n) = \prod_{i<j} \epsilon(x_j - x_i) \tag{6}$$

where $\epsilon(x)$ is the sign function, satisfies

$$\Psi_B(x_1, \ldots, x_n) = A(x_1, \ldots, x_n)\Psi_F(x_1, \ldots, x_n) \tag{7}$$

where Ψ_B is a symmetric wave function for bosons with a hard-core interaction. In the case where Ψ_F is the ground state wave function, this relation simplifies to

$$\Psi_B = |\Psi_F| \tag{8}$$

because the bose ground state must be positive so long as it is not required to vanish by boundary conditions.

Let us first apply this to two spinless particles in a harmonic trap. If $\varphi_j(x)$ is the eigenstate of the j^{th} level of a harmonic oscillator, then the ground state for two fermions is just

$$\Psi_F(x_1, x_2) = \frac{1}{\sqrt{2}}(\varphi_0(x_1)\varphi_1(x_2) - \varphi_0(x_2)\varphi_1(x_1)) = \frac{1}{\sqrt{\pi}} e^{-\frac{1}{2}(x_1^2 + x_2^2)}(x_2 - x_1) \tag{9}$$

and thus by (8)

$$\Psi_B(x_1, x_2) = \frac{1}{\sqrt{\pi}} e^{-\frac{1}{2}(x_1^2 + x_2^2)}|x_2 - x_1| \tag{10}$$

2.3.2 Tan Contact

For two hard-core bosons, we can use (10) to calculate the momentum distribution

$$\begin{aligned} n_B(p) &= \frac{1}{\pi} \int dx \int dx' e^{ip(x-x')} \rho_B(x, x') \\ \rho_B(x, x') &= \frac{1}{\pi} \int dx_2 e^{-\frac{1}{2}(x^2 + x'^2)} e^{-x_2^2} |x_2 - x||x_2 - x'| \end{aligned} \tag{11}$$

For fermions, the momentum distribution will decay exponentially. For HCB this is not the case, however. We showed analytically (using results from [15]) and numerically that

$$\lim_{p \to \infty} n_B(p) = \frac{C_B}{p^4} = \frac{2}{\pi}\sqrt{\frac{2}{\pi}}\frac{1}{p^4} \tag{12}$$

where C_B is known as the momentum tail coefficient or the Tan contact. For an arbitrary number of particles N, the same momentum dependence will hold for large p

$$\lim_{p \to \infty} n_B(p) = \frac{A_N}{p^4} \tag{13}$$

where the Tan contact A_N is a function of the particle number [17]. This asymptotic behavior for $n_B(p)$ will hold for any number of hard-core bosons in a harmonic trap with a finite temperature [25].

2.4 Spinless Anyons

2.4.1 Anyons

In nature, there are two types of particles: bosons and fermions. An important difference between them is that they satisfy different exchange properties, i.e., the former has a symmetric wave function, whereas the latter has an anti-symmetric wave function. A particle known as an anyon satisfies different exchange properties, however. When two anyons are exchanged, the wave function is multiplied by a complex phase factor. For instance, if we represent the wave function for two anyons as $\Psi_\kappa(x_1, x_2)$, then

$$\Psi_\kappa(x_1, x_2) = e^{i\pi\kappa\epsilon(x_1 - x_2)}\Psi_\kappa(x_2, x_1) \tag{14}$$

where $\kappa \in [0, 2)$ is a number known as the anyon statistical parameter and $\epsilon(x)$ is the sign function (positive when $x > 0$, negative when $x < 0$, and zero when $x = 0$). Depending on the value of κ, the anyon will be more like a boson or more like a fermion. Notice, when $\kappa = 0$ the wave function Ψ_κ is symmetric and thus the anyons correspond to bosons. And when $\kappa = 1$ the anyons correspond to fermions because Ψ_κ is antisymmetric.

2.4.2 Anyon-Fermion Mapping

We studied how these results regarding hard-core bosons can be extended to hard-core anyons (HCA). More recently, Girardeau [8] showed that there is an anyon-fermion mapping between hard-core anyons and fermions

$$\begin{aligned} A_\kappa(x_1, \ldots, x_N) &= \prod_{1 \le j < k \le N} e^{i\pi(1-\kappa)\theta(x_k - x_j)} \\ \Psi_\kappa(x_1, \ldots, x_N) &= A_\kappa(x_1, \ldots, x_N)\Psi_F(x_1, \ldots, x_N) \end{aligned} \tag{15}$$

where θ is the Heaviside step function. We can use this tool to answer the same questions about the momentum distribution of HCA.

2.4.3 Tan Contact

Again, we start with the simplest case and consider two hard-core anyons in the ground state of a harmonic trap. Our OBDM is now dependent on κ, thus

$$\rho_\kappa(x, x') = \int dx_2 \cdots dx_N \Psi^*_\kappa(x, \ldots, x_N)\Psi_\kappa(x', \ldots, x_N) \tag{16}$$

where Ψ_κ is obtained via equation (15).

Let $n_\kappa(p)$ be the single particle momentum distribution for anyons with anyon statistical parameter κ (see figure 1 for plots of $n_\kappa(p)$). It can be calculated the same as in the boson case except now using the κ dependent OBDM. We showed numerically and analytically using results from [9, 15] that

$$\lim_{p \to \infty} n_\kappa(p) = \cos^2\left(\frac{\pi\kappa}{2}\right)\frac{C_B}{p^4} \tag{17}$$

For the boson case ($\kappa = 0$), $\cos^2\left(\frac{\pi\kappa}{2}\right) = 1$ and we recover our result from equation (12) for hard-core bosons as we should expect. This Tan contact calculation for anyons can be generalized to an arbitrary number of anyons with a finite temperature and the κ dependence will still be the same [12].

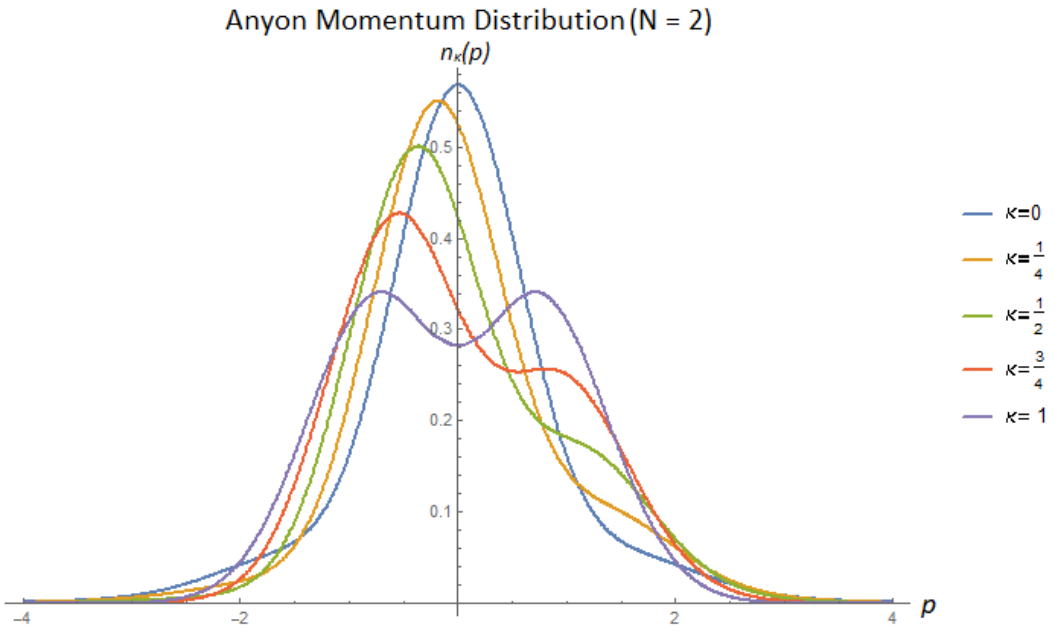

Figure 1: We have used numerical integration to plot $n_\kappa(p)$ for two harmonically-confined, hard-core anyons. The HCB distribution ($\kappa = 0$) is unimodal and displays a fat tail, whereas the fermion distribution ($\kappa = 1$) is bimodal and displays exponential decay.

2.4.4 Dynamical Fermionization

Next, we ask what happens when the trapping potential is turned off at $t = 0$ and the anyon gas is allowed to expand. Equation (1) becomes time dependent

$$H = \sum_i -\frac{1}{2}\frac{\partial^2}{\partial x_i^2} + \frac{1}{2}\omega_i(t)^2 x_i^2 + g\sum_{i<j}\delta(x_i - x_j) \tag{18}$$

where $\omega_i(t) = 1$ for $t \leq 0$ and $\omega_i(t) = 0$ for $t > 0$. Using a scaling transformation [28], the time evolution of each eigenstate in (2) can be solved exactly

$$\begin{aligned} \phi_j(x;t) &= \frac{1}{\sqrt{b}}\phi_j\left(\frac{x}{b};0\right)e^{i\left(\frac{x^2}{2}\frac{\dot{b}}{b} - E_j\tau(t)\right)} \qquad \text{for } j = 0,1,2,\ldots \\ b(t) &= \sqrt{1+t^2} \\ \tau(t) &= \arctan(t) \end{aligned} \tag{19}$$

where E_j is the j^{th} energy level in the harmonic energy spectrum. Equation (19) can be used to derive $\rho_\kappa(x, x'; t)$. Returning to our two anyon case, the time dependent OBDM

$$\rho_\kappa(x, x'; t) = \frac{1}{b}\rho_\kappa\left(\frac{x}{b}, \frac{x'}{b}; 0\right)\exp\left[\frac{i\dot{b}}{2b}(x'^2 - x^2)\right] \tag{20}$$

from which we obtain the momentum distribution

$$n_\kappa(p;t) = \frac{b}{\pi}\int dx \int dx' \rho_\kappa(x, x'; 0)\exp\left[ibp(x - x') + \frac{i\dot{b}b}{2}(x'^2 - x^2)\right] \tag{21}$$

It is difficult to solve this integral exactly. Numerical integration shows that after the trap is turned off the anyon gas will expand and the anyon momentum distribution will approach the fermion distribution. This phenomenon is known as dynamical fermionization (see figure 2). The stationary phase method [1] can be used to show that for any number of particles

$$\lim_{t\to\infty} n_\kappa(p;t) \sim \frac{1}{|\dot{b}|} n_F(p/\dot{b}) \sim n_F(p) \tag{22}$$

where the last equality follows from the fact that b becomes linear for large t [4].

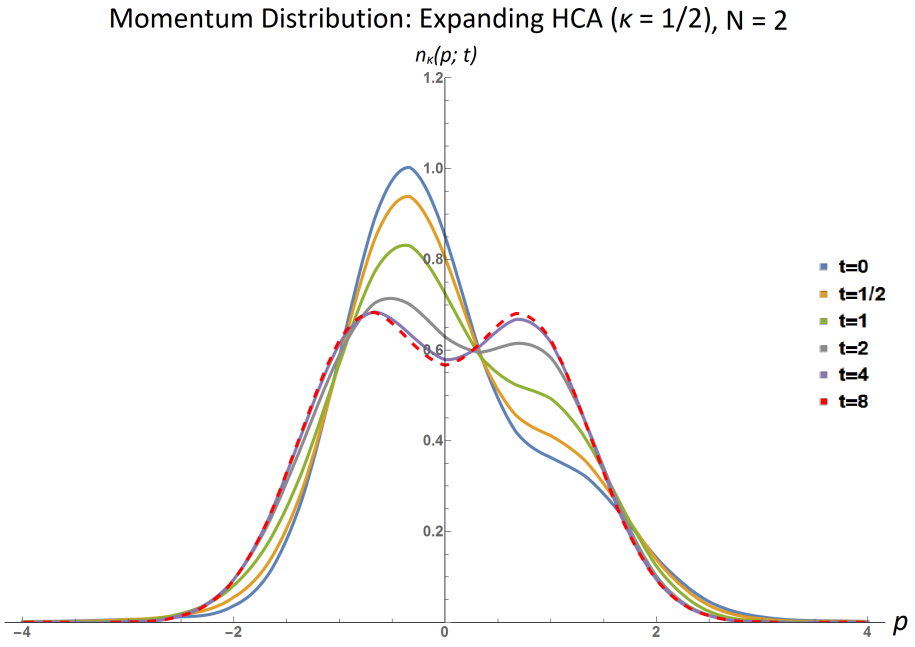

Figure 2: Dynamical fermionization of two hard-core anyons ($\kappa = \frac{1}{2}$) after harmonic trapping potential is turned off at $t = 0$. As t increases, the momentum distribution approaches the fermion distribution.

Figure 1 shows that the fermion distribution has exponential decay whereas the anyon distribution has power law decay. If dynamical fermionization does occur, it must therefore follow that the Tan contact approaches zero in the large t limit. Using the same asymptotic analysis techniques mentioned before, we calculated for the two anyon case

$$\lim_{p\to\infty} n_\kappa(p;t) = \cos^2\left(\frac{\pi\kappa}{2}\right) \frac{C_B}{b^3 p^4} \tag{23}$$

which is zero for the limit $t \to \infty$, as we expected. For larger number of particles, the momentum tail will have the same time dependence [4].

3 Spin Gas

3.1 Background

First we will consider two strongly-interacting bosons with a spin degree of freedom and will calculate whether our results regarding the Tan contact and dynamical fermionization can be generalized to this system as

well. We will assume that the interaction is a spin-independent contact interaction, but no longer hard-core. So the Hamiltonian is still that given in equation (1) but with $g >> 1$ instead of $g \to \infty$.

When g is no longer infinite, the spin of each particle will affect its interaction with other particles. Using second order degenerate perturbation theory, Yang et al. [26] derive a second-order, effective Hamiltonian H_{eff} for spinful fermions in the strongly interacting regime.

$$H_{\text{eff}} = -\frac{1}{g}\sum_{i=1}^{N-1} C_i(1 \pm \mathcal{E}_{i,i+1}) \tag{24}$$

where $\mathcal{E}_{i,i+1}$ is the exchange operator that exchanges the i^{th} particle with the $(i+1)^{th}$ particle. There will be a plus for bosons and minus for fermions. Each C_i is a constant

$$C_i = N\int \prod_j dx_j \left|\frac{\partial \varphi_A}{\partial x_i}\right|^2 \delta(x_{i+1} - x_i)\theta^1_{[i+1,i]} \tag{25}$$

where φ_A is the slater determinant for N spinless fermions, and $\theta^1_{[i+1,i]}$ is the reduced sector function given by

$$\theta^1_{[i+1,i]} = \theta^1/\theta(x_{i+1} - x_i) = \frac{\theta(x_2 - x_1)\cdots\theta(x_N - x_{N-1})}{\theta(x_{i+1} - x_i)}$$

For the spinor case, the OBDM will have a different expression but will follow the same idea that we saw in the spinless case

$$\rho_{\sigma,\sigma'}(x,x') = \sum_{\sigma_2,\ldots,\sigma_N}\int dx_2\cdots dx_N \Psi^*(x,x_2,\ldots,x_N;\sigma,\sigma_2,\ldots,\sigma_N)\Psi(x',x_2,\ldots,x_N;\sigma',\sigma_2,\ldots,\sigma_N) \tag{26}$$

This expression can be rather cumbersome to deal with directly, but for N spinors the corresponding wave function can be generalized to [5, 27]

$$\Psi = \sum_P (\pm 1)^P P[\varphi_A(x_1,\ldots,x_N)\theta^1(x_1,\ldots,x_N)\chi(\sigma_1,\ldots,\sigma_N)] \tag{27}$$

where P is a permutation for that set of indices and ± 1 is for bosons and fermions respectively. This form is also known as the strong coupling ansatz wave function. Starting with this ansatz, Yang et al. [26] simplify the OBDM by separating the spatial and spin components

$$\rho_{\sigma,\sigma'}(x,x') = \sum_{m,n=1}^{N} \rho_{m,n}(x,x')S_{m,n}(\sigma,\sigma') \tag{28}$$

where the spatial component

$$\rho_{m,n}(x,x') = (\pm 1)^{m-n}(N-1)!\int dx_2\cdots dx_N \varphi^*_A\varphi'_A\theta'^{(1,\ldots,m)}\theta^{(1,\ldots,n)} \tag{29}$$

is just the one-body density matrix for the sector $x_2 < x_3 < \cdots < x_m < x' \cdots x_n < x \cdots < x_N$ with $m < n$. Again, the same convention holds for the plus or minus depending on whether the particle is a boson or fermion. The function $\theta^{(1,\ldots,n)}$ refers to a cyclic shift backwards for the first n indices of the sector function θ^1, i.e.,

$$\theta^{(1,\ldots,n)}(x,x_2,\ldots,x_N) = \theta^1(x_2,x_3,\ldots,x_n,x,\ldots,x_N)$$

More generally, the expression $(1,\ldots,n)$ denotes a cyclic permutation on the first n indices

$$x_1,x_2,\ldots,x_N \longrightarrow x_2,x_3,\ldots,x_n,x_1,x_{n+1},\ldots,x_N$$

And the spin component of the one-body density matrix is

$$S_{m,n}(\sigma,\sigma') = [(1,\ldots,m)c_m(\sigma)|\chi\rangle]^\dagger[(1,\ldots,n)c_n(\sigma')|\chi\rangle] \tag{30}$$

where $c_m(\sigma)$ is a destruction operator for the m^{th} particle with spin σ. For instance, $c_2(\frac{1}{2})$ destroys the second particle if it has spin $\frac{1}{2}$. If it does not, then $c_2(\frac{1}{2})\,|\chi\rangle = 0$.

It can be difficult to calculate each C_i, find the eigenstates of H_{eff}, and then evaluate $S_{m,n}(\sigma,\sigma')$, so to help with our future research, we have developed code in Mathematica to calculate each $S_{m,n}$ for arbitrary particle number with arbitrary spin. We have provided an example what this code can do in figure 3.

$$\left[\begin{pmatrix} S_{1,1}(\uparrow,\uparrow) & S_{1,1}(\uparrow,\downarrow) \\ S_{1,1}(\downarrow,\uparrow) & S_{1,1}(\downarrow,\downarrow) \end{pmatrix}\begin{pmatrix} S_{1,2}(\uparrow,\uparrow) & S_{1,2}(\uparrow,\downarrow) \\ S_{1,2}(\downarrow,\uparrow) & S_{1,2}(\downarrow,\downarrow) \end{pmatrix}\begin{pmatrix} S_{1,3}(\uparrow,\uparrow) & S_{1,3}(\uparrow,\downarrow) \\ S_{1,3}(\downarrow,\uparrow) & S_{1,3}(\downarrow,\downarrow) \end{pmatrix}\right.$$
$$\begin{pmatrix} S_{2,1}(\uparrow,\uparrow) & S_{2,1}(\uparrow,\downarrow) \\ S_{2,1}(\downarrow,\uparrow) & S_{2,1}(\downarrow,\downarrow) \end{pmatrix}\begin{pmatrix} S_{2,2}(\uparrow,\uparrow) & S_{2,2}(\uparrow,\downarrow) \\ S_{2,2}(\downarrow,\uparrow) & S_{2,2}(\downarrow,\downarrow) \end{pmatrix}\begin{pmatrix} S_{2,3}(\uparrow,\uparrow) & S_{2,3}(\uparrow,\downarrow) \\ S_{2,3}(\downarrow,\uparrow) & S_{2,3}(\downarrow,\downarrow) \end{pmatrix}$$
$$\left.\begin{pmatrix} S_{3,1}(\uparrow,\uparrow) & S_{3,1}(\uparrow,\downarrow) \\ S_{3,1}(\downarrow,\uparrow) & S_{3,1}(\downarrow,\downarrow) \end{pmatrix}\begin{pmatrix} S_{3,2}(\uparrow,\uparrow) & S_{3,2}(\uparrow,\downarrow) \\ S_{3,2}(\downarrow,\uparrow) & S_{3,2}(\downarrow,\downarrow) \end{pmatrix}\begin{pmatrix} S_{3,3}(\uparrow,\uparrow) & S_{3,3}(\uparrow,\downarrow) \\ S_{3,3}(\downarrow,\uparrow) & S_{3,3}(\downarrow,\downarrow) \end{pmatrix}\right]$$
$$= \left[\begin{pmatrix} \frac{1}{2} & 0 \\ 0 & \frac{1}{2} \end{pmatrix}\begin{pmatrix} \frac{1}{2} & 0 \\ 0 & 0 \end{pmatrix}\begin{pmatrix} 0 & 0 \\ 0 & 0 \end{pmatrix}\right.$$
$$\begin{pmatrix} \frac{1}{2} & 0 \\ 0 & 0 \end{pmatrix}\begin{pmatrix} 1 & 0 \\ 0 & 0 \end{pmatrix}\begin{pmatrix} 0 & 0 \\ 0 & 0 \end{pmatrix}$$
$$\left.\begin{pmatrix} 0 & 0 \\ 0 & 0 \end{pmatrix}\begin{pmatrix} 0 & 0 \\ 0 & 0 \end{pmatrix}\begin{pmatrix} \frac{1}{2} & 0 \\ 0 & \frac{1}{2} \end{pmatrix}\right]$$

Figure 3: Example of calculation for $S_{m,n}(\sigma,\sigma')$ when $|\chi\rangle = \frac{1}{\sqrt{2}}(|\downarrow,\uparrow,\uparrow\rangle - |\uparrow,\uparrow,\downarrow\rangle)$. Each submatrix is a different value of m,n and within each submatrix is a different value for σ,σ'.

3.2 Spin-Independent Interaction

3.2.1 Example: Triplet State

For the case of two spin-$\frac{1}{2}$ bosons, we can see that the eigenstates of the effective Hamiltonian in equation (24) are just the states $|\chi\rangle$ that are symmetric under particle exchange. These eigenstates correspond to the total spin states for two spin-$\frac{1}{2}$ particles.

We will first consider the case where we have two strongly-interacting bosons with total spin state $|\chi\rangle = |S=1,M=1\rangle = |\uparrow,\uparrow\rangle$. First we calculate the spin component of the OBDM. It is immediately apparent that $c_m(\sigma')\,|\chi\rangle$ will be zero unless $\sigma' = \uparrow$, because that is the spin of both particles. For any $m,n \in \{1,2\}$

$$S_{m,n}(\sigma',\sigma) = \begin{cases} 1 & \sigma = \sigma' = \uparrow \\ 0 & \text{else} \end{cases} \tag{31}$$

and thus our one-body density matrix is

$$\rho_{\uparrow,\uparrow}(x,x') = \rho_{1,1}(x,x') + \rho_{1,2}(x,x') + \rho_{2,1}(x,x') + \rho_{2,2}(x,x') \tag{32}$$

We therefore need only calculate the four spatial sectors for the one-body density matrix. Using expression (9) for our slater determinant, we simplify the spatial sectors for the OBDM

$$\rho_{1,1}(x,x') = \frac{1}{\pi}\int_{\max(x',x)}^{\infty} dx_2 e^{-\frac{1}{2}(x^2+x'^2)} e^{-x_2^2}(x_2-x')(x_2-x)$$
$$\rho_{2,2}(x,x') = \frac{1}{\pi}\int_{-\infty}^{\min(x',x)} dx_2 e^{-\frac{1}{2}(x^2+x'^2)} e^{-x_2^2}(x_2-x')(x_2-x)$$

And we can write the sum of the other two as

$$\begin{aligned}\rho_{1,2}(x,x') + \rho_{2,1}(x,x') &= \frac{1}{\pi}\epsilon(x-x')\int_{x'}^{x} dx_2 e^{-\frac{1}{2}(x^2+x'^2)} e^{-x_2^2}(x'-x_2)(x_2-x) \\ &= \frac{1}{\pi}\int_{\min(x',x)}^{\max(x',x)} dx_2 e^{-\frac{1}{2}(x^2+x'^2)} e^{-x_2^2}(x'-x_2)(x_2-x)\end{aligned}$$

We can turn the sum of these terms into a single integral by noting that for each integral, the integrand is always positive, thus

$$\rho_{\uparrow,\uparrow}(x,x') = \frac{1}{\pi}\int dx_2 e^{-\frac{1}{2}(x^2+x'^2)} e^{-x_2^2}|x_2-x'||x_2-x| \tag{33}$$

which is the same OBDM for two spinless, hard-core bosons we saw in (11). So the Tan contact will be the same for $n_{\uparrow,\uparrow}(p)$ as in the spinless case

$$\lim_{p\to\infty} n_{\uparrow,\uparrow}(p) = \frac{C_B}{p^4} = \frac{2}{\pi}\sqrt{\frac{2}{\pi}}\frac{1}{p^4} \tag{34}$$

like in (12). For $|\chi\rangle = |1,0\rangle = \frac{1}{\sqrt{2}}(|\uparrow,\downarrow\rangle + |\downarrow,\uparrow\rangle)$ or $|\chi\rangle = |1,-1\rangle$, the OBDM will take the same form as (33) and at most differ by a constant.

3.2.2 Example: Inseparable Wave Function

For our previous choice of $|\chi\rangle$, the connection to spinless HCB follows quite naturally from the fact that the total wave function for these systems has the same spatial component as the wave function for spinless HCB. For instance, in the case $|\chi\rangle = |\uparrow,\uparrow\rangle$ the total wave function can be written

$$\Psi(x_1,x_2;\sigma_1,\sigma_2) = \Psi_B(x_1,x_2)\otimes\chi(\sigma_1,\sigma_2) \tag{35}$$

where Ψ_B is given by (10) and $\chi(\sigma_1,\sigma_2) = \langle\sigma_1,\sigma_2|\chi\rangle$. In more complicated cases, where the spatial component cannot be separated from the spin component, this connection with spinless HCB is not guaranteed.

The total wave function may not necessarily be separable in this way, however. For instance, consider the following total wave function

$$\Psi(x_1,x_2;\sigma_1,\sigma_2) = \frac{1}{\sqrt{2}}\left[\varphi_F(x_1,x_2)\chi_S(\sigma_1,\sigma_2) + \varphi_B(x_1,x_2)\chi_T(\sigma_1,\sigma_2)\right] \tag{36}$$
$$|\chi_S\rangle = \frac{1}{\sqrt{2}}(|\uparrow,\downarrow\rangle - |\downarrow,\uparrow\rangle)$$
$$|\chi_T\rangle = \frac{1}{\sqrt{2}}(|\uparrow,\downarrow\rangle + |\downarrow,\uparrow\rangle)$$

where Ψ_F and Ψ_B are given in equations (9) and (10) respectively and χ_T and χ_S are the well known triplet and singlet states. Each spin component of this wave function will have non-trivial contributions to its density profile in real space and momentum space.

Due to the simple nature of this example, we can calculate the density profiles and other quantities of interest directly from the full expression for the OBDM

$$\rho_{\sigma,\sigma'}(x,x') = \sum_{\sigma_2,\ldots,\sigma_N} \int dx_2 \cdots dx_N \Psi^*(x,x_2,\ldots,x_N;\sigma,\sigma_2,\ldots,\sigma_N)\Psi(x',x_2,\ldots,x_N;\sigma',\sigma_2,\ldots,\sigma_N)$$

and show that the Tan contact will ultimately still be the same.

$$\begin{aligned}\rho_{\sigma,\sigma'}(x,x') &= \frac{1}{2}\sum_{\sigma_2}\int dx_2 \left[\varphi_F\chi_S + \varphi_B\chi_T\right]\left[\varphi'_F\chi'_S + \varphi'_B\chi'_T\right] \\ &= \frac{1}{2}\sum_{\sigma_2}\int dx_2 \varphi_B\varphi'_B\chi_T\chi'_T + \varphi_B\varphi'_F\chi_T\chi'_S + \varphi_F\varphi'_B\chi_S\chi'_T + \varphi_F\varphi'_F\chi_S\chi'_S \end{aligned} \tag{37}$$

Each spin combination can be simplified greatly

$$\begin{aligned} S_1(\sigma,\sigma') &\equiv \sum_{\sigma_2}\chi_T(\sigma,\sigma_2)\chi_T(\sigma',\sigma_2) = \sum_{\sigma_2}\chi_S(\sigma,\sigma_2)\chi_S(\sigma',\sigma_2) \\ S_2(\sigma,\sigma') &\equiv \sum_{\sigma_2}\chi_T(\sigma,\sigma_2)\chi_S(\sigma',\sigma_2) = \sum_{\sigma_2}\chi_S(\sigma,\sigma_2)\chi_T(\sigma',\sigma_2) \\ S_1(\sigma,\sigma') &= \begin{cases} \frac{1}{2} & \sigma' = \sigma = \uparrow \\ \frac{1}{2} & \sigma' = \sigma = \downarrow \\ 0 & \text{else} \end{cases} \\ S_2(\sigma,\sigma') &= \begin{cases} \frac{1}{2} & \sigma' = \sigma = \uparrow \\ -\frac{1}{2} & \sigma' = \sigma = \downarrow \\ 0 & \text{else} \end{cases} \end{aligned} \tag{38}$$

For each of the four spatial terms in the OBDM ($\varphi_B\varphi'_B$, $\varphi_B\varphi'_F$, ...), they will have their own separate contribution to the momentum distribution. The first term will give the normal p^{-4} dependence we saw previously. The last term will decay exponentially because it is just the fermi distribution, and the second and third term will also decay exponentially

$$\begin{aligned}\int dx dx' dx_2 e^{-ip(x'-x)}\varphi_B(x,x_2)\varphi_F(x',x_2) &= \frac{1}{\pi^2}\int dx \int dx' \int dx_2 e^{-ip(x'-x)}e^{-\frac{1}{2}(x^2+x'^2)}e^{-x_2^2}|x_2-x|(x_2-x') \\ &= \frac{1}{\pi^2}\int dx_2 e^{-x_2^2}\int dx' e^{-ipx'}e^{-x'^2/2}(x_2-x')\int dx e^{ipx}e^{-x^2/2}|x_2-x| \\ \lim_{p\to\infty}\int dx e^{ipx}e^{-x^2/2}|x_2-x| &= \frac{-2e^{-\frac{1}{2}x_2^2}}{p^2} \\ \int dx' e^{-ipx'}e^{-x'^2/2}(x_2-x') &= \sqrt{2\pi}e^{-p^2/2}(x_2+ip)\end{aligned}$$

Because the integral with respect to x' decays exponentially with respect to momentum, the term as a whole for $\varphi_B(x,x_2)\varphi_F(x',x_2)$ will not contribute to the Tan contact. The Tan contact will still, therefore, be the same as the spinless case, because the only term that contributes has the same spatial component as spinless HCB. Thus

$$\lim_{p\to\infty} n_\sigma(p) = \frac{1}{2}\left(\frac{2}{\pi}\sqrt{\frac{2}{\pi}}\frac{1}{p^4}\right)S_1(\sigma,\sigma) \tag{39}$$

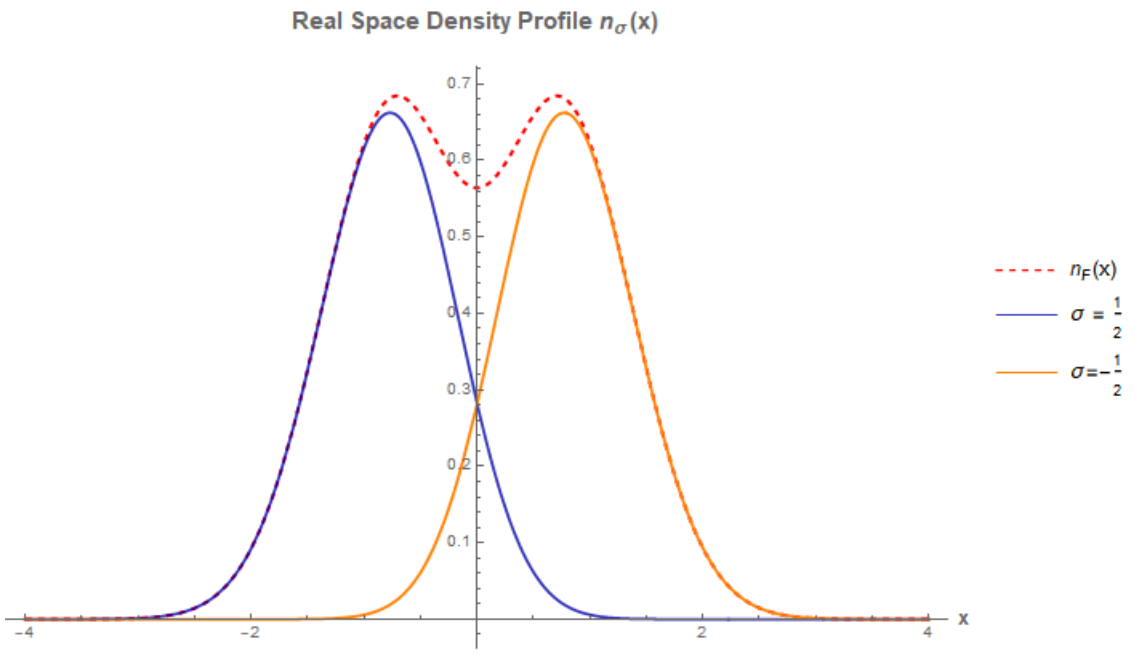

Figure 4: We plot the real space density profile for each value of spin

3.2.2.1 Real Space Density Profile

We will also calculate the time evolution of the momentum distribution after the trap has been turned off, but first lets calculate some other physical characteristics so that we will have something to compare the long-term behavior to. We first calculate the number density in position space

$$\begin{aligned} n_\sigma(x) &= N\rho_{\sigma,\sigma}(x,x) \\ &= \sum_{\sigma_2} \int dx_2 \varphi_B\varphi_B\chi_T\chi_T + \varphi_B\varphi_F\chi_T\chi_S + \varphi_F\varphi_B\chi_S\chi_T + \varphi_F\varphi_F\chi_S\chi_S \end{aligned} \tag{40}$$

where our particle number N is 2, thus eliminating $\frac{1}{2}$. In position space, the boson and fermion solution are the same, so

$$\begin{aligned} n_\sigma(x) &= \frac{1}{2}S_1(\sigma,\sigma)(n_F(x)+n_B(x)) + 2S_2(\sigma,\sigma)\int dx_2\varphi_F(x,x_2)\varphi_B(x,x_2) \\ &= S_1(\sigma,\sigma)n_F(x) + S_2(\sigma,\sigma)\frac{2}{\pi}\int dx_2 e^{-(x^2+x_2^2)}(x_2-x)|x_2-x| \\ &= S_1(\sigma,\sigma)n_F(x) + S_2(\sigma,\sigma)n_C(x) \end{aligned} \tag{41}$$

where $n_F(x)$ is the real space density for two spinless fermions and $n_C(x)$ is the real density profile from the bose-fermi coupled terms in the OBDM

$$n_F(x) = \frac{e^{-x^2}(1+2x^2)}{\sqrt{\pi}} \tag{42}$$

$$n_C(x) = 2\int dx_2\varphi_F(x,x_2)\varphi_B(x,x_2) = \frac{-2xe^{-2x^2} - e^{-x^2}(1+2x^2)\,\mathrm{erf}(x)}{\pi} \tag{43}$$

If we plot (41) for each value of spin σ, we obtain fig. 4

3.2.2.2 Momentum Space Density Profile

Now we consider the density profile in momentum space before the trap has been turned off. We start with the general expression for two particles

$$n_\sigma(p) = \frac{1}{\pi}\int dx \int dx' e^{ip(x-x')}\rho_\sigma(x,x') \tag{44}$$

Plugging in our result from equation (37) and simplifying some, we can express our spin OBDM as

$$\rho_{\sigma,\sigma'}(x,x') = \frac{1}{2}S_1(\sigma,\sigma')(\rho_B(x,x')+\rho_F(x,x'))+\frac{1}{2}S_2(\sigma,\sigma')\left(\int dx_2\varphi_F(x,x_2)\varphi_B(x',x_2)+\varphi_F(x',x_2)\varphi_B(x,x_2)\right) \tag{45}$$

We are familiar with the first two components are standard terms, so we need only examine the calculation for the latter term. We can define our coupled term momentum space density profile as

$$n_C(p) = \frac{1}{2}\frac{N}{2\pi}\int dx_2 \int dx \int dx' e^{ip(x-x')}(\varphi_F(x,x_2)\varphi_B(x',x_2)+\varphi_F(x',x_2)\varphi_B(x,x_2)) \tag{46}$$

It can be shown that this function will be identically zero using a parity argument as follows

$$\begin{aligned}
n_C(p) &= \frac{1}{\pi}\int dx_2 \int dx \int dx' \cos(p(x-x'))\varphi_F(x,x_2)\varphi_B(x',x_2) \\
&= \frac{1}{\pi^2}\int dx_2 \int dx \int dx' \cos(p(x-x'))e^{-\frac{1}{2}(x^2+x'^2)}e^{-x_2^2}(x_2-x)|x_2-x'| \\
&= \frac{1}{\pi^2}\int dx \int dx' \cos(p(x-x'))e^{-\frac{1}{2}(x^2+x'^2)}(-2xe^{-\frac{1}{2}x^2-\frac{3}{2}x'^2}-e^{-\frac{1}{2}(x^2+x'^2)}\sqrt{\pi}(1+2xx')\operatorname{erf}(x'))
\end{aligned}$$

Note that in the last expression the entire integrand picks up a negative sign under the transformation $x \to -x$ and $x' \to -x'$, so we should expect the integral over a symmetric region to be zero. Thus, the momentum space density profile simplifies to

$$n_\sigma(p) = \frac{1}{2}S_1(\sigma,\sigma)(n_B(p)+n_F(p)) \tag{47}$$

a plot of this distribution is given in figure 5.

3.2.2.3 Time Evolution of Density Profiles

Now we turn to the long term dynamics of the momentum space density profile after the trapping potential has been turned off. To find the time evolution of this system, we use a scaling transformation [28]. Our two particle OBDM will evolve as

$$\rho_{\sigma,\sigma'}(x,x';t) = \frac{1}{2b}e^{\frac{ib}{2b}(x'^2-x^2)}\left(\left(\rho_B\left(\frac{x}{b},\frac{x'}{b};0\right)+\rho_F\left(\frac{x}{b},\frac{x'}{b};0\right)\right)S_1+\left(\rho_C\left(\frac{x}{b},\frac{x'}{b};0\right)+x\leftrightarrow x'\right)S_2\right) \tag{48}$$

where our scaling function $b(t) = \sqrt{1+t^2}$ and

$$\rho_C(x,x';0) \equiv \int dx_2\varphi_F(x,x_2)\varphi_B(x',x_2)$$

and the momentum space density profile is

$$n_\sigma(p;t) = \frac{1}{\pi}\int dx \int dx' e^{ip(x-x')}\rho_\sigma(x,x';t) \tag{49}$$

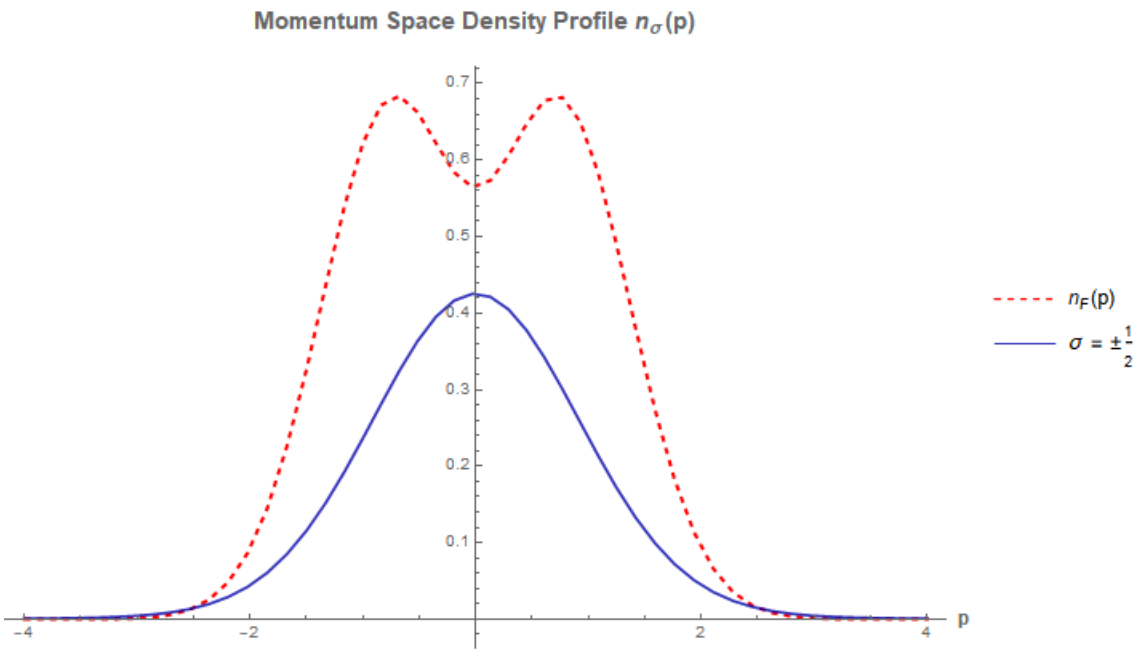

Figure 5: Plot of momentum space density profile for (36)

Because our OBDM can be separated into OBDM for other systems we have already studied, our expression for the momentum space density profile can be decomposed as follows

$$n_\sigma(p;t) = \frac{1}{2}\left(n_B(p;t) + n_F(p;t)\right) S_1 + n_C(p;t) S_2 \tag{50}$$

where

$$n_C(p;t) \equiv \frac{1}{2\pi b}\int dx \int dx' e^{ip(x-x')} e^{\frac{ib}{2b}(x'^2-x^2)} \left(\rho_C\left(\frac{x}{b},\frac{x'}{b};0\right) + x \leftrightarrow x'\right) \tag{51}$$

Switching the integration labels around, we can simplify this integral to find that

$$n_C(p;t) \equiv \frac{1}{\pi b}\int dx \int dx' \cos\left(p(x-x') + \frac{\dot{b}}{2b}(x'^2 - x^2)\right) \rho_C\left(\frac{x}{b},\frac{x'}{b};0\right) \tag{52}$$

Notice that under the transformation $x \to -x$ and $x' \to -x'$, the integrand does not change sign due to the $(x'^2 - x^2)$ term. The integrand is no longer odd, so we cannot use a parity argument like we did in equation (46) to show the integral vanishes. In fact, the integral will be non-zero.

Separating the momentum density profiles in equation (50) makes it easier to find the $t \to \infty$ behavior because it has already been shown [16] that

$$\lim_{t\to\infty} n_B(p;t) = n_F(p) = \frac{e^{-p^2}(1+2p^2)}{\sqrt{\pi}} \tag{53}$$

and the fermi distribution does not change when the trap is turned off. Thus, we only need to find the large t behavior of $n_C(p;t)$. We can simplify the expression for $n_C(p;t)$ to obtain

$$\begin{aligned}\frac{1}{2\pi b}\int dx \int dx' e^{ip(x-x')} e^{\frac{ib}{2b}(x'^2-x^2)} \rho_C\left(\frac{x}{b},\frac{x'}{b};0\right) &= \frac{b}{2\pi}\int dx_2 \int dx \int dx' e^{ibp(x-x')} e^{\frac{ibb}{2}(x'^2-x^2)} \varphi_F(x,x_2)\varphi_B(x',x_2) \\ &= \frac{b}{2\pi^2}\int dx_2 \int dx \int dx' e^{ibp(x-x')} e^{\frac{ibb}{2}(x'^2-x^2)} e^{-\frac{1}{2}(x^2+x'^2)} e^{-x_2^2}(x_2-x)|x_2-x'|\end{aligned}$$

Then, using the stationary phase approximation we find that

$$\lim_{t\to\infty} n_C(p;t) = \frac{-2pe^{-2p^2} - e^{-p^2}(1+2p^2)\sqrt{\pi}\,\mathrm{erf}(p)}{\pi} \tag{54}$$

which is the same function as the real space density profile from equation (43). In conclusion, the large t behavior is therefore

$$\lim_{t\to\infty} n_\sigma(p;t) = S_1(\sigma,\sigma)n_F(p) + S_2(\sigma,\sigma)\frac{-2pe^{-2p^2} - e^{-p^2}(1+2p^2)\sqrt{\pi}\,\mathrm{erf}(p)}{\pi} \tag{55}$$

This result has been plotted in figure 6, thus obtaining the same profile as we observed in the real space density profile prior to expansion. It also follows from equation (38) and (55) that

$$\lim_{t\to\infty} \sum_\sigma n_\sigma(p;t) = n_F(p) \tag{56}$$

We can therefore conclude that dynamical fermionization can occur in spinful systems and that each spin component can contribute to the overall momentum distribution in a non-trivial fashion.

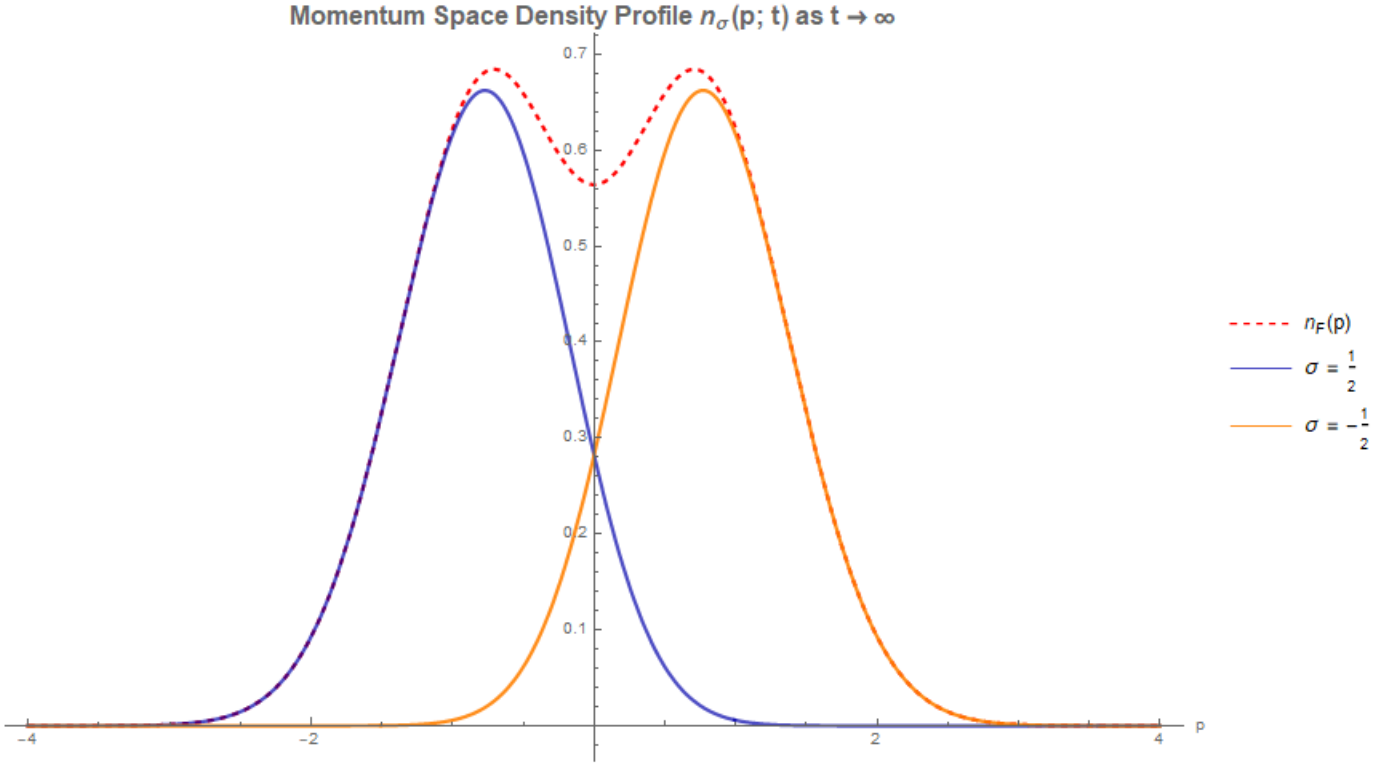

Figure 6: Here is a plot of the momentum space density profile after the trap has been turned off and $t \to \infty$

Notice that after the trapping potential has been turned off, the $\sigma = \frac{1}{2}$ particle has a predominantly negative momentum, whereas the $\sigma = -\frac{1}{2}$ particle tends to have a positive momentum. If this is the case, we should expect to see in the RSDP for both these particles that the $\sigma = \frac{1}{2}$ particle moves to the left and the $\sigma = -\frac{1}{2}$ moves to the right. Let's calculate this to check our result.

The time dependent RSDP is given by

$$n_\sigma(x;t) = N\rho_{\sigma,\sigma}(x,x;t) \tag{57}$$

and using equation (48), we obtain the expression

$$n_\sigma(x;t) = \frac{1}{b}\left(S_1 n_F\left(\frac{x}{b};0\right) + S_2 n_C\left(\frac{x}{b};0\right)\right) \tag{58}$$

and these two functions are given analytically in equations (42) and (43) respectively. We have created an animation of the time evolution of this RSDP, and our numerical calculation confirms that the two particles will move away from one another.

We can plot the location of the two modes in the RSDP (one mode for the density profile of each σ) as a function of time to illustrate this more clearly (fig. 7). As a confirmation of these results, we should see that the derivative of the position curve for each of these density peaks, should approach the final momentum of each particle after dynamical fermionization has occurred. Because the final MSDP is the same distribution as the initial RSDP however, this just means that the intial value of each density peak should approximately equal the steady state slope of each density peak trajectory.

In other words, if we denote $Q_\sigma(t)$ as the location of the RSDP mode for the particle with spin σ, then our previous analysis translates to the statement

$$Q_\sigma(0) = \lim_{t\to\infty} Q'_\sigma(t)$$

Numerical calculations confirm this with $Q_\sigma(0) \approx .771242$ and the best fit line for $Q_\sigma(t)$ in interval $t \in [100, 150]$ has slope $m = 0.771217$. This calculation is a nice indirect result of the dynamical fermionization already discussed.

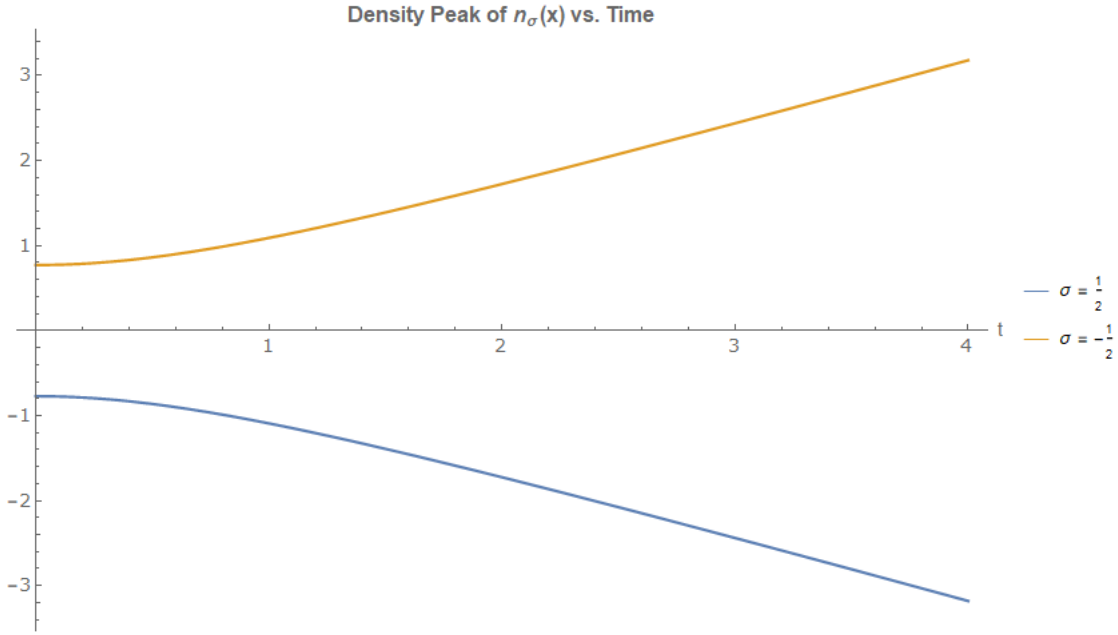

Figure 7: This is a plot of the time evolution of the two modes in $n_\sigma(x)$ for each σ after the trapping potential has been turned off. The two peaks move away from each other and approach a constant momentum.

3.3 N Particle Spin Gas

These past examples have illustrated that the phenomenon of dynamical fermionization is by no means constrained to spinless systems, and can occur in strongly-interacting spin gases. Indeed, it can be shown

that dynamical fermionization will occur in a strongly-interacting spin gas of any particle number, even if it has a spin-dependent interaction. In this section, we have reproduced a proof of this fact below that was found by Shah Saad Alam using results from Li Yang.

To calculate the long-term dynamics of a spin gas after the trapping potential has been turned off, we must first solve for $\rho_{\sigma,\sigma'}(x,x';t)$. Recall that we can write the OBDM with the form

$$\rho_{\sigma,\sigma'}(x,x';t) = \sum_{m,n} \rho_{m,n}(x,x';t) S_{m,n}(\sigma,\sigma') \tag{59}$$

If we consider the case where $g \to \infty$, the spin components will not evolve and we need only calculate the dynamics of the spatial components $\rho_{m,n}(x,x';t)$. Using our expression in equation (19) for the time dependence of individual eigenstates after the quench, we can write the time evolution of the entire slater determinant to be

$$\varphi_A(x_1,...,x_N;t) = b^{-N/2}\varphi_A\left(\frac{x_1}{b},...,\frac{x_N}{b};0\right)\exp\left[i\frac{\dot{b}}{2b}\sum_{j=1}^{N}x_j^2 - i\tau\sum_{j=1}^{N}E_j\right] \tag{60}$$

where $b(t)$ and $\tau(t)$ are defined in (19). If we substitute this expression into the equation for $\rho_{m,n}$ and simplify the integrals, we find that

$$\rho_{m,n}(x,x';t) = \frac{1}{b}\exp\left[\frac{i\dot{b}}{2b}(x'^2 - x^2)\right]\rho_{m,n}(x/b,x'/b;0) \tag{61}$$

and because the spin components in (59) do not change, we can immediately conclude

$$\rho_{\sigma,\sigma'}(x,x';t) = \frac{1}{b}\exp\left[\frac{i\dot{b}}{2b}(x'^2 - x^2)\right]\rho_{\sigma,\sigma'}(x/b,x'/b;0) \tag{62}$$

allowing us to express the full time dependence of ρ in terms of its initial value. The MSDP for these spinors is

$$n_{\sigma,\sigma'}(p;t) = \frac{1}{2\pi b}\int dx' \int dx\ \rho_{\sigma,\sigma'}(x/b,x'/b;0)\exp\left[ip(x-x') + \frac{i\dot{b}}{2b}(x'^2 - x^2)\right] \tag{63}$$

using a change of variables in the integral

$$n_{\sigma,\sigma'}(p;t) = \frac{b}{2\pi}\int dx' \int dx\ \rho_{\sigma,\sigma'}(x,x';0)\exp\left[ib\left(p(x-x') + \frac{\dot{b}}{2}(x'^2 - x^2)\right)\right] \tag{64}$$

In the limit where $t \to \infty$, we also have $b \to \infty$, so we can apply the stationary phase approximation as before

$$\lim_{t\to\infty} n_{\sigma,\sigma'}(p;t) = \frac{1}{|\dot{b}|}\rho_{\sigma,\sigma'}\left(\frac{p}{\dot{b}},\frac{p}{\dot{b}};0\right) \tag{65}$$

Writing out $\rho_{\sigma,\sigma'}\left(\frac{p}{\dot{b}},\frac{p}{\dot{b}};0\right)$ we see that

$$\begin{aligned}\rho_{\sigma,\sigma'}\left(\frac{p}{\dot{b}},\frac{p}{\dot{b}};0\right) &= \sum_{m,n}\rho_{m,n}\left(\frac{p}{\dot{b}},\frac{p}{\dot{b}};0\right)S_{m,n}(\sigma,\sigma') \\ &= \sum_{m}\rho_{m,m}\left(\frac{p}{\dot{b}},\frac{p}{\dot{b}};0\right)S_{m,m}(\sigma,\sigma')\end{aligned}$$

where the last equality follows from the fact that when $x = x'$, $\rho_{m,n}(x,x')$ will be zero when $m \neq n$ due to the heaviside theta terms in (29). So,

$$\lim_{t\to\infty} n_{\sigma,\sigma'}(p;t) = \frac{1}{|\dot{b}|}\sum_{m}\rho_{m,m}\left(\frac{p}{\dot{b}},\frac{p}{\dot{b}};0\right)S_{m,m}(\sigma,\sigma') \tag{66}$$

To see the significance of this result, consider the case where the gas is spin polarized and thus $S_{m,m}(\sigma_0, \sigma_0) = 1$. Then,

$$\lim_{t\to\infty} n_{\sigma_0,\sigma_0}(p;t) = \frac{1}{|\dot{b}|}\sum_m \rho_{m,m}\left(\frac{p}{\dot{b}}, \frac{p}{\dot{b}}; 0\right) = \frac{1}{|\dot{b}|}\rho_F\left(\frac{p}{\dot{b}}, \frac{p}{\dot{b}}\right) \tag{67}$$

where ρ_F is the OBDM for the slater determinant. It is also known that for fermions at zero temperature [10] the MSDP will be the same as the OBDM

$$n_F(p) = \rho_F(p,p) \tag{68}$$

Alam concludes

$$\lim_{t\to\infty} n_{\sigma_0,\sigma_0}(p;t) = \frac{1}{|\dot{b}|}n_F\left(\frac{p}{\dot{b}}\right) \tag{69}$$

Again, in the large t limit, b becomes linear and $\dot{b} \to 1$. It is therefore manifest that the total momentum distribution for this spin polarized case will undergo dynamical fermionization.

In the more general case where the gas is not spin polarized, we can see from (66) that each component of spin will contribute to the overall MSDP in a non-trivial way.

4 Anharmonic Trapping Potentials

In the results that we have discussed, we have explored the phenomenon of dynamical fermionization and how it emerges in different harmonically confined systems. In this investigation, we have had to define more clearly what the phenomenon really is and what it means for the phenomenon to occur in systems that are not spinless. It nonetheless remained unclear what property of these systems was necessary for dynamical fermionization to occur.

For instance, there existed a duality between the real space and momentum space distributions that originated from the harmonic potential Hamiltonian

$$\hat{H} = \frac{\hat{p}^2}{2} + \frac{\hat{x}^2}{2} \tag{70}$$

and its property that it is symmetric under exchange $p \leftrightarrow x$. When this is the case, an eigenstate projected onto the position basis will have the same profile as an eigenstate projected onto the momentum basis. This was the reason for the correspondence between the MSDP for spinless fermions and the RSDP for other strongly-interacting particles.

The harmonic potential also had the special property that the eigenstates for a Hamiltonian with time-varying trapping frequency could be solved analytically, and in the case where the trapping potential was quenched, the eigenstates would undergo a self-similar transformation as seen in equations (19) and (48).

Was it one of these properties that caused strongly-interacting particles (irrespective of spin) in harmonic traps dynamically fermionize? Was it a property of the trapping potential? If it was not, can we formulate more general conditions for its presence?

In the following sections we will try to address some of these questions. Our numerical results show that dynamical fermionization will occur when particles have been confined in anharmonic traps, even if the trapping potentials are not symmetric. First, we will discuss the numerical methods we used to reach these results, and then we will discuss in how these results can be understood on a more theoretical basis.

4.1 General Formulation

Recall our previous investigation of dynamical fermionization of strongly-interacting, spinless bosons. We assumed that two spinless bosons were confined in a harmonic trap, and we calculated the long-term dynamics of the MSDP in the scenario where the trapping potential is turned off. Now we would like to consider the effects of adding anharmonicity to the Hamiltonian, thus giving

$$H = -\frac{1}{2}\frac{\partial^2}{\partial x^2} + \frac{1}{2}x^2 + \alpha x^3 + \lambda x^4 \tag{71}$$

We will assume that the parameters α and λ can be treated as perturbation parameters. Let $\phi_0^{(0)}, \phi_1^{(0)}, \ldots$ denote eigenstates of the unperturbed Hamiltonian (the Hamiltonian with harmonic only harmonic potential) and let $\phi_0, \phi_1, \ldots$ denote the eigenstates the Hamiltonian with anharmonicity included.

First, we will use the Imaginary Time Propagation (ITP) method to compute the new ground state and first excited state for two fermions [3, 18]. This method involves making the substitution $t \to -i\tau$ in the Schrodinger equation. The resulting equation will be a real, diffusive PDE

$$\frac{\partial \psi}{\partial \tau} = \frac{1}{2}\frac{\partial^2 \psi}{\partial x^2} - V(x)\psi \tag{72}$$

By numerically solving this PDE with an initial condition (or trial function) that is not orthogonal to the ground state, we will eventually arrive at a numerical representation of the ground state over a given region. We used the Backward Euler numerical scheme to solve (72). Please see the cited references for more explanation of this method.

In our case, we must find the ground state $\phi_0(x)$ as well as the first excited state $\phi_1(x)$. We can still use ITP to do this if we choose a trial function that is orthogonal to the ground state. For instance, when H commutes with parity, this can be accomplished by choosing an odd trial function, because the ground state is guaranteed to be even. When $\alpha \neq 0$ in equation (71), this will not work because the eigenstates of the Hamiltonian will no longer be simultaneous eigenstates with the parity operator.

To get around this, we numerically calculate $\phi_0(x)$ in an anharmonic potential and then $\phi_1^{(0)}$ under the L^2 inner product. Because we consider α and λ perturbation parameters, $\phi_1^{(0)}$ should still be close to $\phi_1(x)$. The resulting wave function will be orthogonal to $\phi_0(x)$ by construction, and as it evolves under equation (72) it will tend to maintain this orthogonality. If the ITP algorithm ever starts failing to maintain this orthogonality (which empirically turned out to be the case for some trapping potentials), the orthogonality condition can be reinforced by performing an additional orthogonal projection every 10-30 iterative steps of the ITP method.

Once we have these eigenstates in position space $\phi_0(x)$ and $\phi_1(x)$, we can calculate how they will evolve in time by projecting them onto the plane-wave basis for the free-particle Hamiltonian. When the trapping potential has been turned off, the new Hamiltonian for these fermions will be

$$\hat{H} = \frac{\hat{p}^2}{2} \tag{73}$$

whose eigenstates $|\phi_p\rangle$ are just the momentum space basis, i.e., $|\phi_p\rangle = |p\rangle$. The time evolution of $\phi_0(x)$ and

$\phi_1(x)$ is therefore

$$\begin{aligned}
\phi_0(x,t) &= \langle x|\phi_0(t)\rangle \\
&= \int dp\, \langle x|\phi_p\rangle \langle \phi_p|\phi_0(t)\rangle \\
&= \int dp\, \langle x|p\rangle \langle p|\phi_0(t)\rangle \\
&= \int dp\, e^{ipx} \langle p|e^{-i\hat{H}t}|\phi_0(0)\rangle \\
&= \int dp\, e^{ipx} \langle p|\phi_0(0)\rangle e^{-i\frac{p^2}{2}t} \\
&= \int dp\, e^{ipx} \widetilde{\phi_0}(p) e^{-i\frac{p^2}{2}t}
\end{aligned} \tag{74}$$

where $\widetilde{\phi_0}(p)$ is $\phi_0(x)$ in the momentum basis. This provides a numerically convenient way of computing dynamics of the eigenstates after the quench. From here, the procedure for testing for dynamical fermionization is fairly similar to the methodology used elsewhere in this thesis. Once $\phi_0(x,t)$ and $\phi_1(x,t)$ have been calculated, we can find the slater determinant $\varphi_A(x_1,x_2;t)$ and hence the wave function Ψ_B for two strongly-interacting, spinless bosons using the Bose-Fermi mapping. To determine whether dynamical fermionization occurs, we calculate the OBDM with Ψ_B and then use that to find

$$n(p;t) = \frac{N}{2\pi} \int dx \int dx' e^{ip(x-x')} \rho(x,x';t) \tag{75}$$

4.2 Numerical Results

4.2.1 Ground State & First Excited State

First, we will consider the case where $\alpha = 0$ and $\lambda = 0.1$. Figures 8 and 9 plot the resulting ground state and first excited state. For reference, we have also plotted the corresponding unperturbed eigenstate for each case.

To ensure that these computed eigenstates are correct, we compute the energy of the trial wave function at each iteration to ensure that it is indeed decreasing. To make the convergence easier to plot for each eigenstate, we have subtracted the final energy value from the energy value at each iteration of the trial wave function, which is why both curves appear to converge to zero in the plot. Figure 10 shows that energy is converging with this method.

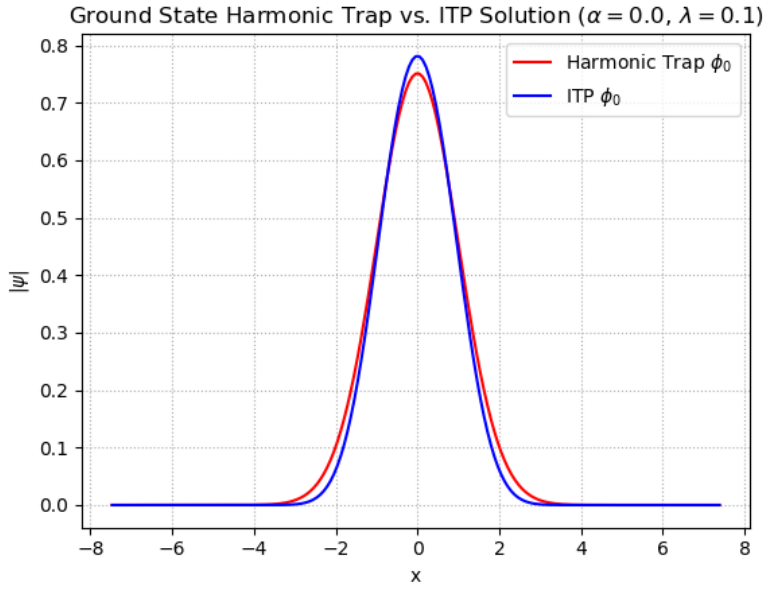

Figure 8: Ground state wave function for anharmonic potential. Computed ϕ_0 is the anharmonic wave function "computed" from the ITP method. The red plot depicts the ground state for harmonic potential.

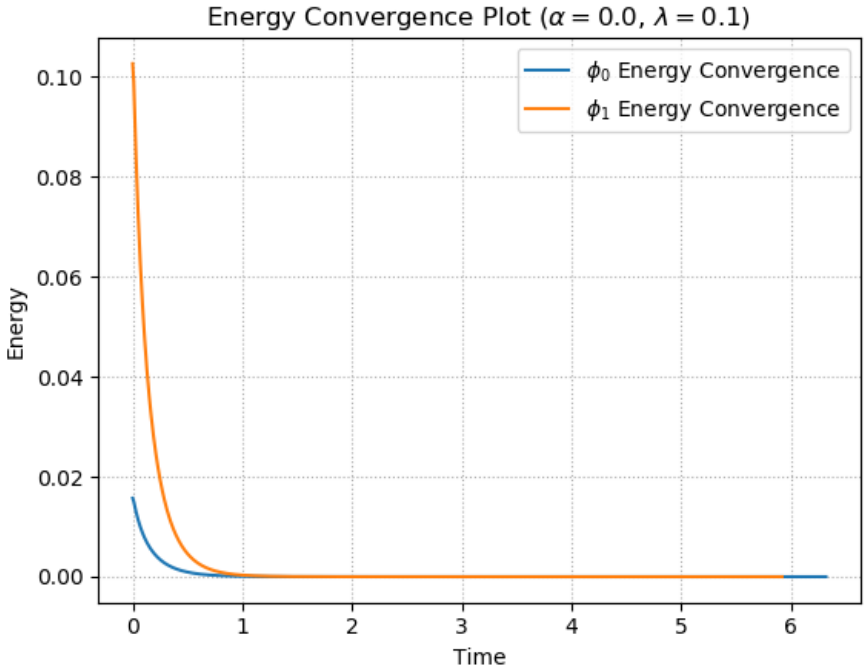

Figure 10: At every tenth time step of the ITP method, we have recorded the energy of the trial solution. For this plot, we recorded the energy at different iterations and subtracted the final energy the method converged to. Thus, these plots merely show the relationship between the initial energy of the trial function and the energy of successive iterations.

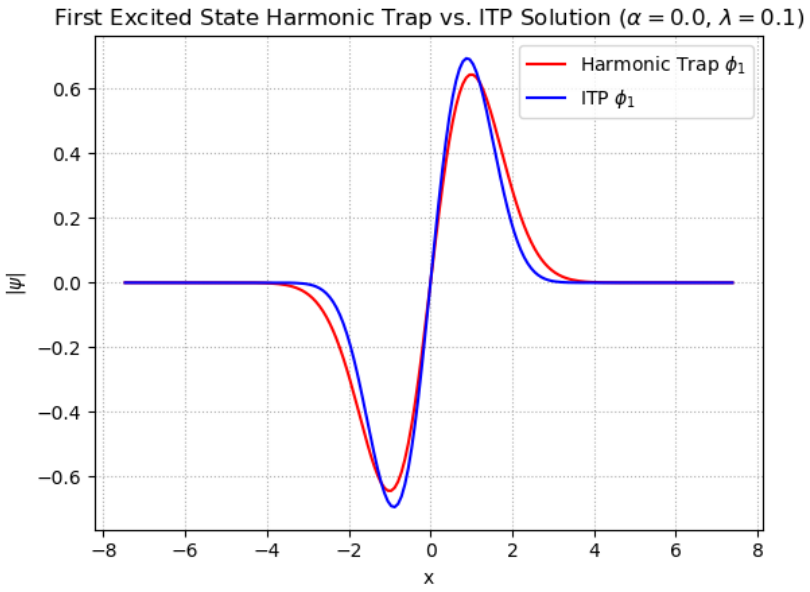

Figure 9: First excited state for anharmonic potential. Labeling convention is same as in previous plot.

4.2.2 One Body Density Matrix and Momentum Space Density Profile

After obtaining the eigenstates, we transform these wave functions to find their representation in momentum space. We calculated the momentum distribution $\widetilde{\phi}_i(p)$ of each of these eigenstates and have plotted $\widetilde{\phi_0}(p)$ in figure 11.

By using equation (74), we can calculate the time evolution of each eigenstate in the situation where both trapping potentials are suddenly turned off. Then, $\phi_i(x,t)$ can be used to compute $\rho_B(x,x';t)$ by using the bose-fermi mapping on the slater determinant.

Again, when $\lambda = 0$, the OBDM can be calculated analytically and compared to our computed values. We did this to check our code and found that our computed OBDM for a harmonic potential differed from the exact answer by an average value of 10^{-5}. To check the validity of this time evolution method, we also made sure that the particle number of the RSDP is conserved through time, which we have plotted in figure **??**

Figure 12 depicts how the RSDP is affected by the addition of the quartic potential term to the Hamiltonian. Of course, the question we are really interested in is what happens to the MSDP after all trapping potentials are turned off? Even when the quartic perturbation is added to the Hamiltonian, we still see dynamical fermionization occur. Figure 13 shows that the MSDP at $t = 6$ (orange figure) is almost identical to the initial MSDP of non-interacting fermions in an anharmonic potential (purple).

For reference,we have also plotted other relevant momentum space density profiles that are very similar. The green figure plots the initial RSDP of the harmonically confined bosons. Because the quartic perturbation breaks the symmetry between momentum space and position space, the initial RSDP and final MSDP are different now. Nonetheless, the plot shows that as the time t increases, the bosonic MSDP asymptotically approaches the fermi MSDP

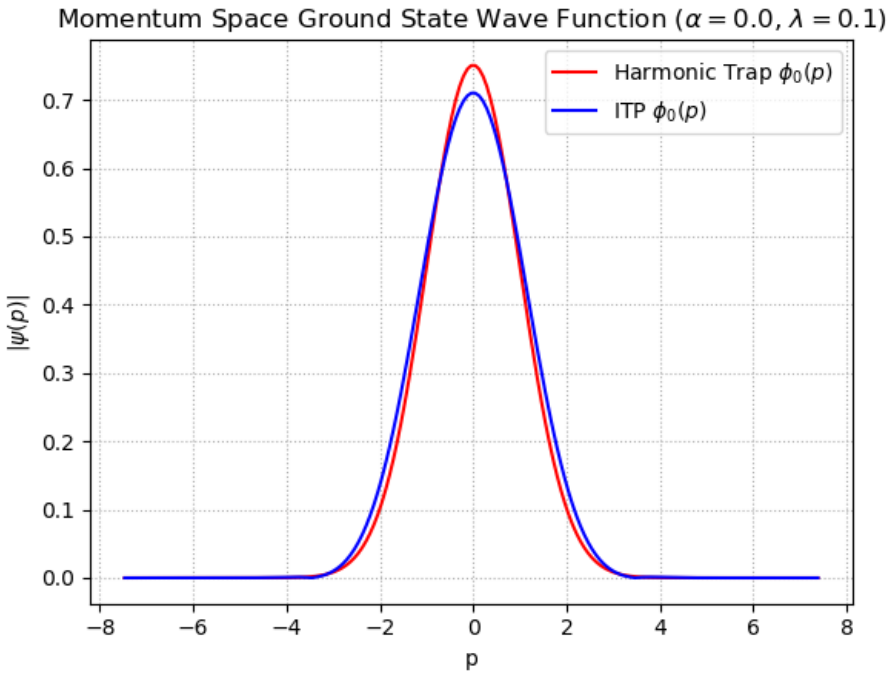

Figure 11: Momentum distribution for ground state wave function.

4.2.3 Asymmetric Anharmonicity

It is rather surprising to find that dynamical fermionization will still occur even when the bosons are not harmonically confined. But now we ask, what factor does the symmetry of the Hamiltonian play in this? Because the parity operator commutes with Hamiltonian in equation (71) when $\alpha = 0$, the resulting eigenstates are symmetric. When $\alpha \neq 0$, our eigenstates of the Hamiltonian will no longer be eigenstates of the parity operator, so we will have asymmetric eigenfunctions. We now numerically consider the long term dynamics for the case where $\lambda = 0.05$ and $\alpha = 0.1$. The ground state and first excited state are no longer even/odd with this potential, and as a result the initial RSDP is no longer symmetric either (figure 14)

Nonetheless, the momentum space density profile remains even, and we still observe dynamical fermionization in this trapping potential.

4.3 Analytic Approach

Admittedly, it is rather curious to see the asymmetric RSDP juxtaposed with the completely symmetric time evolution of the MSDP, but this can be explained. Recalling our expression for the real space density profile

$$n(x) = N\rho(x,x) = \int dx_2 \Psi^*(x,x_2)\Psi(x,x_2) \tag{76}$$

the symmetry of this expression under the exchange $x \to -x$ is completely dependent on the eigenstates of our Hamiltonian, which make up the slater determinant $\Psi(x_1,x_2)$. In general, $\Psi(x_1,x_2)$ is only symmetric under exchange $x_1 \to x_2$, which is guaranteed by our bose-fermi mapping of the slater determinant. Total wave function $\Psi(x_1,x_2)$ will have parity symmetry when the eigenstates $\phi_0(x)$ and $\phi_1(x)$ that comprise it

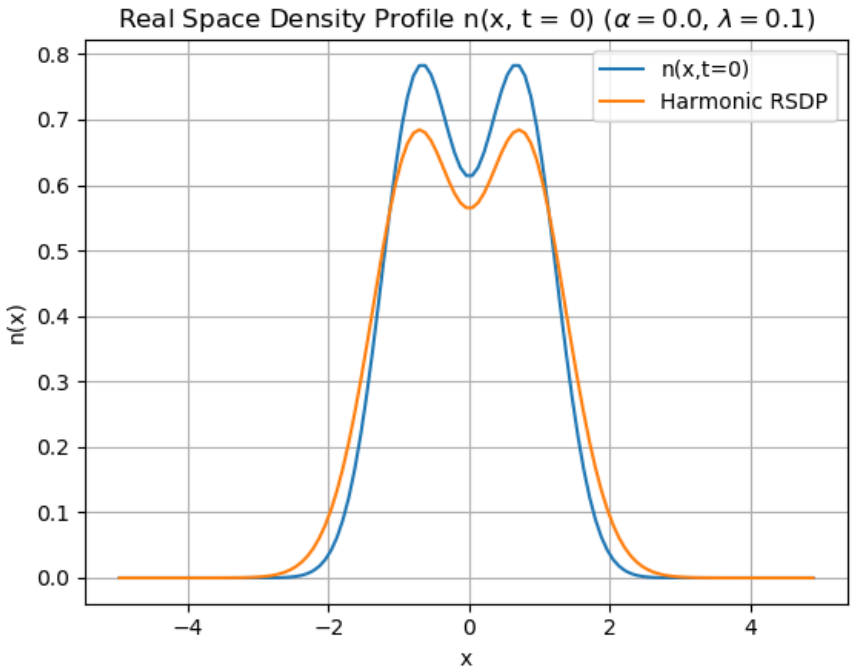

Figure 12: RSDP before the trapping potential is turned off ($\lambda = 0.1$). The blue figure is the anharmonic RSDP and the orange figure is the RSDP for two harmonically confined fermions.

have parity symmetry.

This symmetry came from the fact that the parity operator $\hat{\Pi}$ commuted with the Hamiltonian in equation (71), which meant that our eigenstates were degenerate in the parity subspace. Once we know this to be true, an arbitrary eigenbasis $\phi_0, \phi_1, \ldots$ for the Hamiltonian can simultaneously be eigenstates of $\hat{\Pi}$. If the Hamiltonian in equation (71) does not have this symmetry when $\alpha \neq 0$, then why is the MSDP even? The MSDP is even because the eigenstates $\phi_n(p)$ in momentum space satisfy $\widetilde{\phi_n}(p) = \widetilde{\phi_n}^*(-p)$. To see this, observe that at $t = 0$ we have

$$\widetilde{\phi_n}(p) = \frac{1}{\sqrt{2\pi}} \int dx e^{-ipx} \phi_n(x) \tag{77}$$

Because $\phi_n(x)$ is real at this time, we can see that taking the complex conjugate of this expression would have the same effect as letting $p \to -p$. Hence, $\widetilde{\phi_n}(p) = \widetilde{\phi_n}^*(-p)$. Defining $\widetilde{\Psi}(q, q') = \frac{1}{\sqrt{2}} \left(\widetilde{\phi_0}(q) \widetilde{\phi_1}(q') - \widetilde{\phi_0}(q') \widetilde{\phi_1}(q) \right)$, we can write the MSDP

$$n(p; 0) = N \int dp_2 \widetilde{\Psi}^*(p, p_2) \widetilde{\Psi}(p, p_2) \tag{78}$$

and see that exchanging $p \to -p$ and taking the complex conjugate will leave it unchanged. Thus, $n(p; 0)$ will always be even.

We now would like to ask whether the dynamical fermionization results can be justified on a more

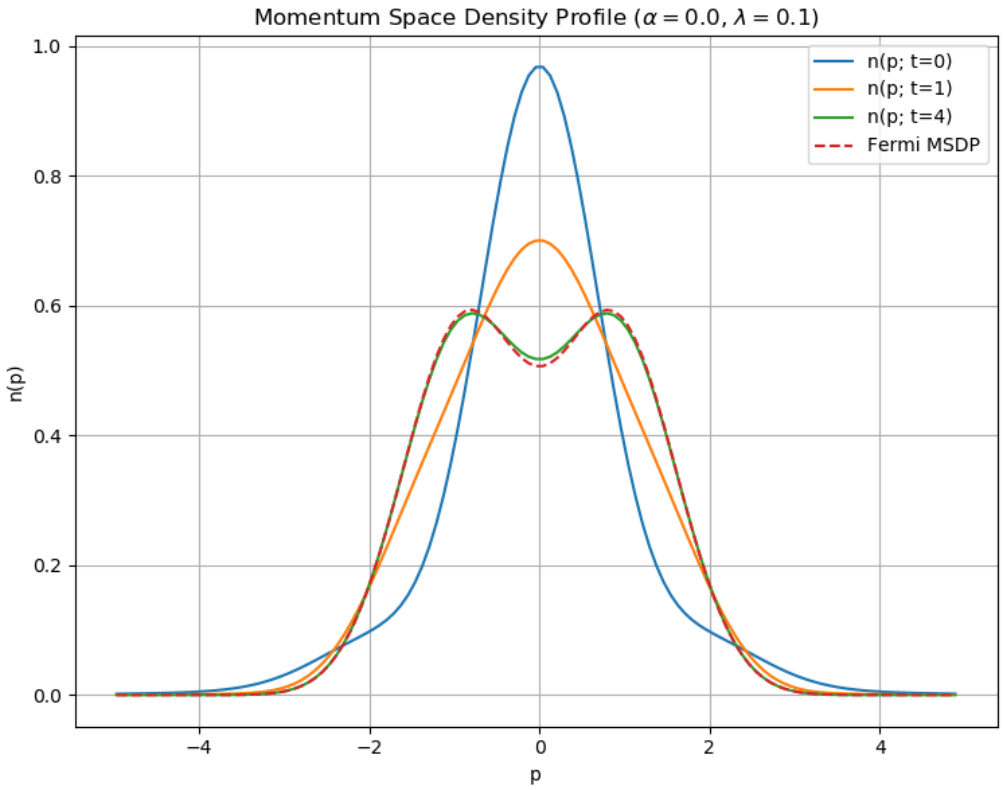

Figure 13: This figure plots $n(p;t)$, for the anharmonically confined bosons at different times. Fermi MSDP is the MSDP of fermions with the anharmonic potential.

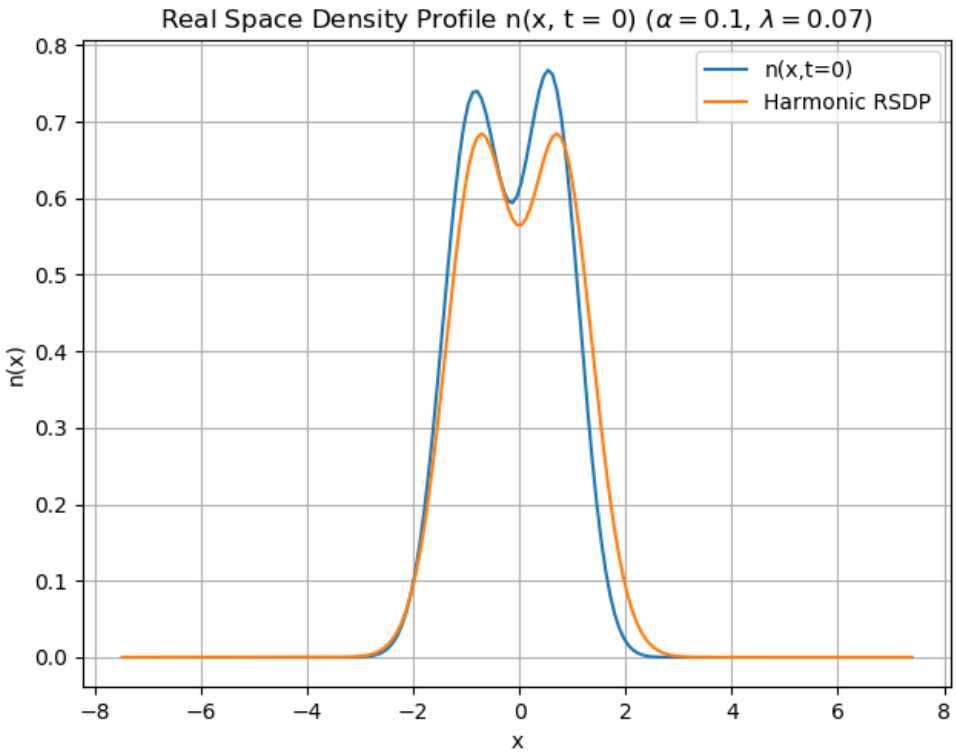

Figure 14: This figure plots the initial real space density profile for the case of an asymmetric trapping potential

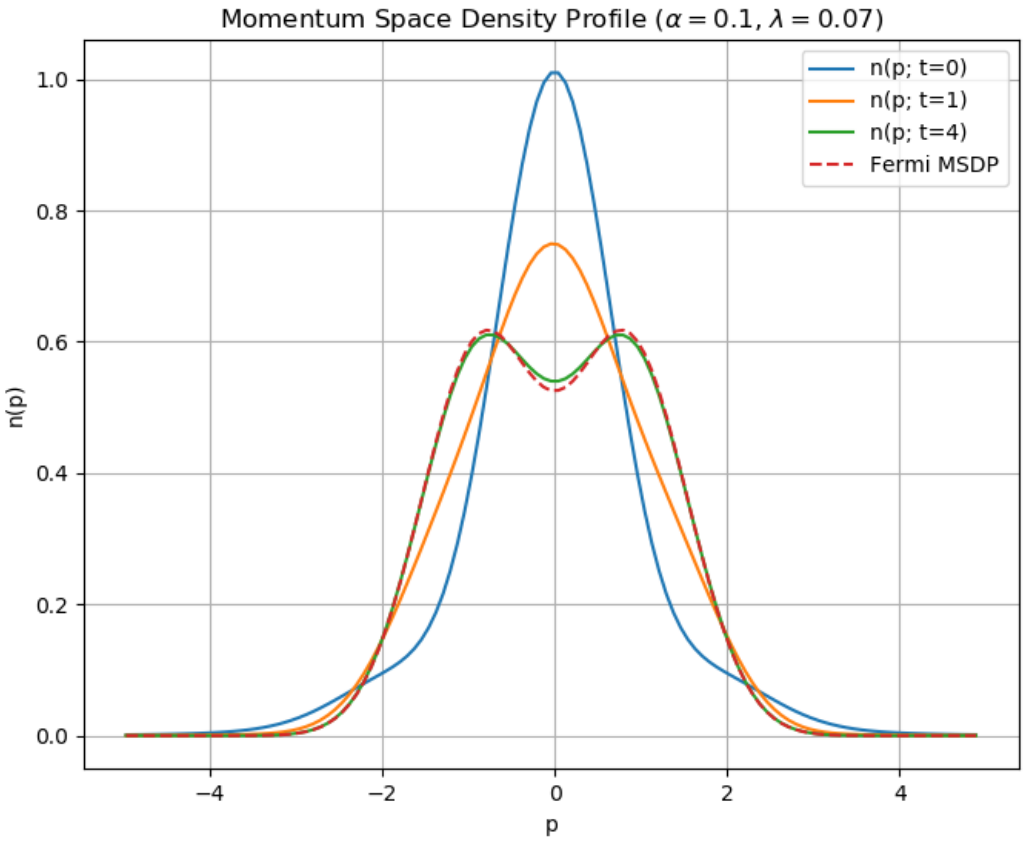

Figure 15: This figure plots the MSDP for various situations. We can see that the final MSDP of the strongly interacting spinless bosons approaches the momentum distribution of spinless fermions.

theoretical basis. We start with equation (75) to obtain

$$\begin{aligned} n(p;t) &= \frac{N}{2\pi}\int dx \int dx' e^{ip(x-x')}\rho(x,x';t) \\ &= \frac{N}{2\pi}\int dx \int dx \int dx_2 e^{ip\left(x-x'\right)}\Psi_F^*\left(x,x_2;t\right)\Psi_F\left(x',x_2;t\right)\epsilon\left(x_2-x\right)\epsilon\left(x_2-x'\right) \\ &= \frac{N}{2\pi}\int dx_2 \left|\int dx e^{-ipx}\epsilon\left(x_2-x\right)\Psi_F\left(x,x_2;t\right)\right|^2 \end{aligned}$$

We can substitute in an expression for Ψ_F in terms of the eigenstates in momentum space

$$\begin{aligned} \Psi_F\left(x_1,x_2;t\right) &= \frac{1}{\sqrt{2}}\left(\phi_0\left(x_1;t\right)\phi_1\left(x_2;t\right)-\phi_0\left(x_2;t\right)\phi_1\left(x_1;t\right)\right) \\ &= \frac{1}{\sqrt{2}}\frac{1}{2\pi}\int dq\int dq' \exp\left[iqx_1+iq'x_2-\frac{i}{2}\left(q^2+q'^2\right)t\right]\left(\widetilde{\phi_0}(q)\widetilde{\phi_1}\left(q'\right)-\widetilde{\phi_0}\left(q'\right)\widetilde{\phi_1}(q)\right) \\ &= \frac{1}{2\pi}\int dq\int dq' \exp\left[iqx_1+iq'x_2-\frac{i}{2}\left(q^2+q'^2\right)t\right]\widetilde{\Psi}\left(q,q'\right) \end{aligned} \tag{79}$$

Plugging (79) back into our expression for the MSDP and using u-substitution to replace $x-x_2$ with x

$$\begin{aligned} n(p;t) &= \frac{N}{(2\pi)^3}\int dx_2 \left|\int dx\int dq\int dq'\epsilon\left(x-x_2\right)\exp\left[i(q-p)x+iq'x_2-\frac{i}{2}\left(q^2+q'^2\right)t\right]\widetilde{\Psi}\left(q,q'\right)\right|^2 \\ &= \frac{N}{(2\pi)^3}\int dx_2 \left|\int dx\int dq\int dq'\epsilon\left(x\right)\exp\left[i(q-p)x+i(q'+q-p)x_2-\frac{i}{2}\left(q^2+q'^2\right)t\right]\widetilde{\Psi}\left(q,q'\right)\right|^2 \end{aligned}$$

and we can see that the integral over the variable x is just a fourier transform of the sign function $\epsilon(x)$. From [15] we know that

$$\frac{1}{\sqrt{2\pi}}\int_{-\infty}^{\infty}\epsilon(x)e^{ipx}dx = \frac{i\sqrt{\frac{2}{\pi}}}{p} \tag{80}$$

thus the MSDP becomes

$$n(p;t) = 4\frac{N}{(2\pi)^3}\int dx_2 \left|\int dq\int dq' \exp\left[i(q'+q)x_2-\frac{i}{2}\left(q^2+q'^2\right)t\right]\frac{1}{q-p}\widetilde{\Psi}\left(q,q'\right)\right|^2$$

Now looking at the integral over q, it is tempting to try and evaluate it as a contour integral. A standard way of doing this is to move the pole from p to $p+i\epsilon$ and then evaluate a contour integral with a half-moon shape on the positive imaginary axis. The $i\epsilon$ term moves the pole off the real line, and so the contour integral can be evaluated as the combination of an integral over the real line and a half-circle integral with constant R like so

$$\oint_C f(z)dz = \int_{-R}^{R} f(z)dz + \int_{\text{Arc}} f(z)dz \tag{81}$$

and then the real line integral can be easily solved for by taking $R\to\infty$. The arc integral is zero in many cases by Jordan's Lemma, which states that the arc integral will approach zero as $R\to\infty$ if $f(Re^{i\theta})$ approaches zero uniformly with θ. To show this is satisfied in this case, we would have to make certain assumptions about the asymptotic expression for $\widetilde{\Psi}\left(q,q'\right)$. One choice would be to assume that

$$\widetilde{\Psi}\left(q,q'\right)\to P(q,q')e^{-q^2} \tag{82}$$

where $P(q,q')$ is some polynomial function. Unfortunately, any choice of gaussian decay would not allow us to satisfy Jordan's lemma because this would cause the integrand to exponentially grow along the imaginary axis. If this assumption about the asymptotic expression for $\widetilde{\Psi}(q,q')$ can be justified, it may be possible to get around this difficulty with Jordan's Lemma by making a variable substitution $q=\sqrt{u}$. This would make the contour integral much more difficult because it would require us to make a branch cut in the complex plane.

Nonetheless, there may be another avenue to simplifying this integral if we evaluate the integral with respect to x_2, noticing that this is just a dirac delta function.

$$\begin{aligned}
n(p;t) &= 4\frac{N}{(2\pi)^3}\int dx_2 \int d^4\vec{q}\exp\left[i\left(q_1+q_2-q_3-q_4\right)x_2 - \frac{i}{2}\left(q_1^2+q_2^2-q_3^2-q_4^2\right)t\right] \\
&\qquad\qquad \times \frac{1}{q_1-p}\frac{1}{q_3-p}\widetilde{\Psi}\left(q_1,q_2\right)\widetilde{\Psi}^*\left(q_3,q_4\right) \\
&= 4\frac{N}{(2\pi)^3}\sqrt{2\pi}\int d^4\vec{q} \quad \delta(q_1+q_2-q_3-q_4)\exp\left[-\frac{i}{2}\left(q_1^2+q_2^2-q_3^2-q_4^2\right)t\right] \\
&\qquad\qquad \times \frac{1}{q_1-p}\frac{1}{q_3-p}\widetilde{\Psi}\left(q_1,q_2\right)\widetilde{\Psi}^*\left(q_3,q_4\right) \\
&= 4\frac{N}{(2\pi)^3}\sqrt{2\pi}\int d^3\vec{q} \quad \exp\left[-\frac{i}{2}\left(q_1^2+q_2^2-q_3^2-(q_1+q_2-q_3)^2\right)t\right]\frac{1}{q_1-p}\frac{1}{q_3-p}\widetilde{\Psi}\left(q_1,q_2\right)\widetilde{\Psi}^*\left(q_3,q_1+q_2-q_3\right) \\
&= 4\frac{N}{(2\pi)^3}\sqrt{2\pi}\int d^3\vec{q} \quad \exp\left[-i(q_1-q_3)(q_3-q_2)t\right]\frac{1}{q_1-p}\frac{1}{q_3-p}\widetilde{\Psi}\left(q_1,q_2\right)\widetilde{\Psi}^*\left(q_3,q_1+q_2-q_3\right)
\end{aligned}$$

Applying the stationary phase approximation in this situation is not straightforward because there is a not a finite set of critical points for this phase function.

5 Conclusion

References

[1] N. Bleistein and R. A. Handelsman. *Asymptotic expansions of integrals*. Courier Corporation, 1986.

[2] F. Camino, W. Zhou, and V. Goldman. Realization of a laughlin quasiparticle interferometer: Observation of fractional statistics. *Physical Review B*, 72(7):075342, 2005.

[3] M. L. Chiofalo, S. Succi, and M. Tosi. Ground state of trapped interacting bose-einstein condensates by an explicit imaginary-time algorithm. *Physical Review E*, 62(5):7438, 2000.

[4] A. Del Campo. Fermionization and bosonization of expanding one-dimensional anyonic fluids. *Physical Review A*, 78(4):045602, 2008.

[5] F. Deuretzbacher, K. Fredenhagen, D. Becker, K. Bongs, K. Sengstock, and D. Pfannkuche. Exact solution of strongly interacting quasi-one-dimensional spinor bose gases. *Physical review letters*, 100(16):160405, 2008.

[6] M. Girardeau. Relationship between systems of impenetrable bosons and fermions in one dimension. *Journal of Mathematical Physics*, 1(6):516–523, 1960.

[7] M. Girardeau. Permutation symmetry of many-particle wave functions. *Physical Review*, 139(2B):B500, 1965.

[8] M. Girardeau. Anyon-fermion mapping and applications to ultracold gases in tight waveguides. *Physical review letters*, 97(10):100402, 2006.

[9] M. Girardeau, E. Wright, and J. Triscari. Ground-state properties of a one-dimensional system of hard-core bosons in a harmonic trap. *Physical Review A*, 63(3):033601, 2001.

[10] F. Gleisberg, W. Wonneberger, U. Schlöder, and C. Zimmermann. Noninteracting fermions in a one-dimensional harmonic atom trap: Exact one-particle properties at zero temperature. *Physical Review A*, 62(6):063602, 2000.

[11] D. J. Griffiths and D. F. Schroeter. *Introduction to quantum mechanics*. Cambridge University Press, 2018.

[12] Y. Hao and Y. Song. One-dimensional hard-core anyon gas in a harmonic trap at finite temperature. *The European Physical Journal D*, 71(6):135, 2017.

[13] T. Kinoshita, T. Wenger, and D. S. Weiss. Observation of a one-dimensional tonks-girardeau gas. *Science*, 305(5687):1125–1128, 2004.

[14] E. H. Lieb and W. Liniger. Exact analysis of an interacting bose gas. i. the general solution and the ground state. *Physical Review*, 130(4):1605, 1963.

[15] M. J. Lighthill. *An introduction to Fourier analysis and generalised functions*. Cambridge University Press, 1958.

[16] A. Minguzzi and D. Gangardt. Exact coherent states of a harmonically confined tonks-girardeau gas. *Physical review letters*, 94(24):240404, 2005.

[17] A. Minguzzi, P. Vignolo, and M. Tosi. High-momentum tail in the tonks gas under harmonic confinement. *Physics Letters A*, 294(3-4):222–226, 2002.

[18] P. Muruganandam and S. K. Adhikari. Fortran programs for the time-dependent gross–pitaevskii equation in a fully anisotropic trap. *Computer Physics Communications*, 180(10):1888–1912, 2009.

[19] B. Paredes, P. Fedichev, J. Cirac, and P. Zoller. 1 2-anyons in small atomic bose-einstein condensates. *Physical review letters*, 87(1):010402, 2001.

[20] B. Paredes, A. Widera, V. Murg, O. Mandel, S. Fölling, I. Cirac, G. V. Shlyapnikov, T. W. Hänsch, and I. Bloch. Tonks–girardeau gas of ultracold atoms in an optical lattice. *Nature*, 429(6989):277, 2004.

[21] M. Rigol and A. Muramatsu. Fermionization in an expanding 1d gas of hard-core bosons. *Physical review letters*, 94(24):240403, 2005.

[22] S. Tan. Energetics of a strongly correlated fermi gas. *Annals of Physics*, 323(12):2952–2970, 2008.

[23] S. Tan. Generalized virial theorem and pressure relation for a strongly correlated fermi gas. *arXiv preprint arXiv:0803.0841*, 2008.

[24] S. Tan. Large momentum part of a strongly correlated fermi gas. *Annals of Physics*, 323(12):2971–2986, 2008.

[25] P. Vignolo and A. Minguzzi. Universal contact for a tonks-girardeau gas at finite temperature. *Physical review letters*, 110(2):020403, 2013.

[26] L. Yang, L. Guan, and H. Pu. Strongly interacting quantum gases in one-dimensional traps. *Physical Review A*, 91(4):043634, 2015.

[27] L. Yang and H. Pu. One-body density matrix and momentum distribution of strongly interacting one-dimensional spinor quantum gases. *Physical Review A*, 95(5):051602, 2017.

[28] Y. B. Zel'dovich et al. *Quantum mechanics: selected topics*. World Scientific, 1998.

[29] W. Zwerger. *The BCS-BEC crossover and the unitary Fermi gas*, volume 836. Springer Science & Business Media, 2011.